Energy Conversion and Management: X 23 (2024) 100657

Contents lists available at ScienceDirect

Energy Conversion and Management: X

journal homepage: www.sciencedirect.com/journal/energy-conversion-and-management-x

Optimisation and control of tidal range power plants operation: Is there scope for further improvement?

Agustina Skiarski [a,*], Nicolás Faedo [b], John V. Ringwood [a]

[a] Centre for Ocean Energy Research, Department of Electronic Engineering, Maynooth University, Maynooth, Co. Kildare, Ireland
[b] Marine Offshore Renewable Energy Lab, Department of Mechanical and Aerospace Engineering, Politecnico di Torino, Torino, Italy

ARTICLE INFO

Keywords:
Tidal energy
Tidal barrages
Ocean energy
Control
Optimisation
Tidal barrage operation

ABSTRACT

Tidal barrage power plants utilise the tidal range variation to generate clean electricity. Although there are several operating tidal barrage schemes around the globe, there is still potential to expand the installed capacity. Given their inherent storage and the high predictability of the tides, tidal barrages can be operated with more flexibility than many other renewables. This means that the control objective of a barrage operation can vary from energy maximisation to constant power output, or demand-matching objectives. The operation of a barrage also influences its impact on the environment and economic activity of the site where it is located, which is a major cause for the slow deployment of such power plants. The aim of this study is to provide a comprehensive and critical analysis of the different strategies considered to date to optimise the operation of tidal barrages, with a focus on an in-depth analysis of the optimisation schemes employed, the barrage models utilised, and opportunities for further improvement.

1. Introduction

The energy sector worldwide is moving towards clean and renewable sources, driven by the growing concern regarding the environmental impact and economic volatility of fossil fuels. Some technologies, such as wind and solar, have reached a high level of commercial/economic maturity, and are currently considered safe investments. Nevertheless, these intermittent and low-inertia sources present considerable challenges to power grids as their level of penetration increases. In 2022, the European Commission proposed to increase the EU 2030 target of 40% of energy consumption from renewable sources to 45% [1]. Achieving this goal will intrinsically require to include a wider range of renewable technologies in the energy mix.

Ocean energy, on the other hand, has had a slower development than other sister renewables, yet presents considerable potential for accelerating the energy transition. In particular, tidal energy is more predictable and less intermittent than solar or wind, as the resource has a periodic behaviour that can be accurately forecasted years in advance.

There are two energy sources that can be harnessed from the tides: the tidal range and the tidal currents. The tidal range is the difference between high seawater and low seawater, generated by the change in tidal height in a site. The tidal current is the horizontal movement of seawater that accompanies the rise and fall of the sea surface. Tidal barrages generate electrical power using the potential energy from the tidal range, while tidal stream turbines use the kinetic energy from the tidal currents.

A tidal barrage scheme consists of an embankment that separates a body of water close to a shore, usually an estuary or bay, from the open sea, creating a reservoir, as seen in Fig. 1. The embankment has a certain number of sluices and turbines to allow the passage of water. As the tide level increases (or decreases), a hydraulic head is created between the basin and the open sea. The potential energy of the water due to this head is converted to mechanical energy through the turbines, which are coupled to electric generators.

Depending on their mode of operation, tidal barrage plants can achieve a certain level of dispatchability, which can complement the more unpredictable wind and solar plants and enhance the robustness of electrical grids. Moreover, the carbon emissions per unit of electricity of tidal barrages are estimated to be close to $10 gCO_2/kWh$, which is similar to that of on-shore wind farms and a third of the emissions per unit electricity of solar PV [2]. Tidal range plants have the advantage of using mature technologies, which has allowed them to reach a commercial stage sooner than other ocean energies. The first large-scale commercial tidal barrage power plant, La Rance (France), started operating in 1966

* Corresponding author.
E-mail addresses: Agustina.Skiarski.2024@mumail.ie (A. Skiarski), nicolas.faedo@polito.it (N. Faedo), John.Ringwood@mu.ie (J.V. Ringwood).

https://doi.org/10.1016/j.ecmx.2024.100657

Available online 5 July 2024

[3], followed by several others, with the newest one being Sihwa Lake Tidal Power Station (South Korea), built in 2011, having the highest tidal barrage installed capacity in the world [4].

In the absence of major technological challenges, the main issues that constrain the deployment of tidal barrage power plants are their high investment cost and their environmental impact [5]. In this sense, optimising the operation of tidal barrage plants is key to ensure that they are economically competitive, while taking into consideration constraints given by the surrounding environment. As discussed within this study (in Section 5), traditionally, the predominant approach pursued in the literature has been on the so-called fixed parameter operation of tidal barrages, where the operational sequence of the turbines and sluice gates of the barrage remains constant, as seen for example in [6], with limited regard to the change in tidal range through each cycle. More recently, several studies proposed more flexible solutions to tidal barrage operation by considering optimal control techniques, with different objective functions, synthesis methods, and associated numerical solvers. For instance, [7] implement gradient-based algorithms to solve the optimal control problem, while [8] apply genetic algorithms, [9] apply particle swarm optimisation, and [10], evolutionary algorithms. Model predictive control [11], moment-based control [12], and reinforcement learning [13] have also been considered. Each study has several simplifying assumptions that partially cover the solution space, leaving room for further research.

Currently, a number of studies exist within the literature that present reviews on different aspects of tidal barrages. [5] provides an overview of the status of the global tidal energy scene, where the issues and perspectives of tidal barrages and tidal turbines are discussed; however, the study dates from 2009 and has not been updated. A more recent review [14] describes different optimisation objectives for tidal barrage operation. [15] describes the different turbines used in tidal barrages and gives a range of possible technologies that could be implemented in future schemes. [16] gives a general perspective on the evolution of modelling and optimisation of tidal lagoons, with a focus on the development of the Swansea Bay Lagoon project. [17] analyses the integration of tidal lagoon schemes in the UK electric system. [18] reviews different optimisation methods applied to tidal barrages, with a focus on hydrodynamic modelling. [19] gives an overview of the impact of tidal energy on water quality. Nonetheless, none of the studies discussed within this paragraph address the major issue of optimisation and control of these technologies, which is fundamental to ensure competitiveness of tidal barrage schemes in an economical sense.

Motivated by the lack of a clear pathway and updated perspectives on tidal barrage optimisation, this paper gives a comprehensive and critical overview of the optimal control problem formulation of tidal barrage operation, providing a detailed analysis of the current literature. The different models, objective functions, manipulated variables, strategies, and algorithms implemented are described, with views on gaps, challenges and opportunities in the study of operational optimisation of tidal barrages, placing specific emphasis on future directions that need to be taken in order to push research towards effective and efficient optimal control and optimisation of these assets.

The remainder of the paper is organised as follows. Section 2 gives an overview of the tidal resource and its distribution around the world. Section 3 describes the types of barrages and their operational modes, and documents the existing tidal barrage power plants that currently operate in the world. Section 4 details various mathematical modelling options for tidal barrages and Section 5 reviews the existing control and optimisation techniques found in literature. The conclusions, with perspectives for future work on tidal barrage operation, are outlined in Section 6.

2. The tidal range energy resource

This section describes the phenomena that cause the tides and the analytical representation of tidal variations, and gives an overview of the tidal range resource around the world. In particular, Section 2.1 discusses tidal variations, while Section 2.2 provides a detailed account on the global tidal range resource.

2.1. Models for tidal variations

Tides are a result of the gravitational interaction between the Earth, the Moon and the Sun, which produces a periodic rise and fall of the mean sea surface. This phenomenon is based on Newton's law of gravitation:

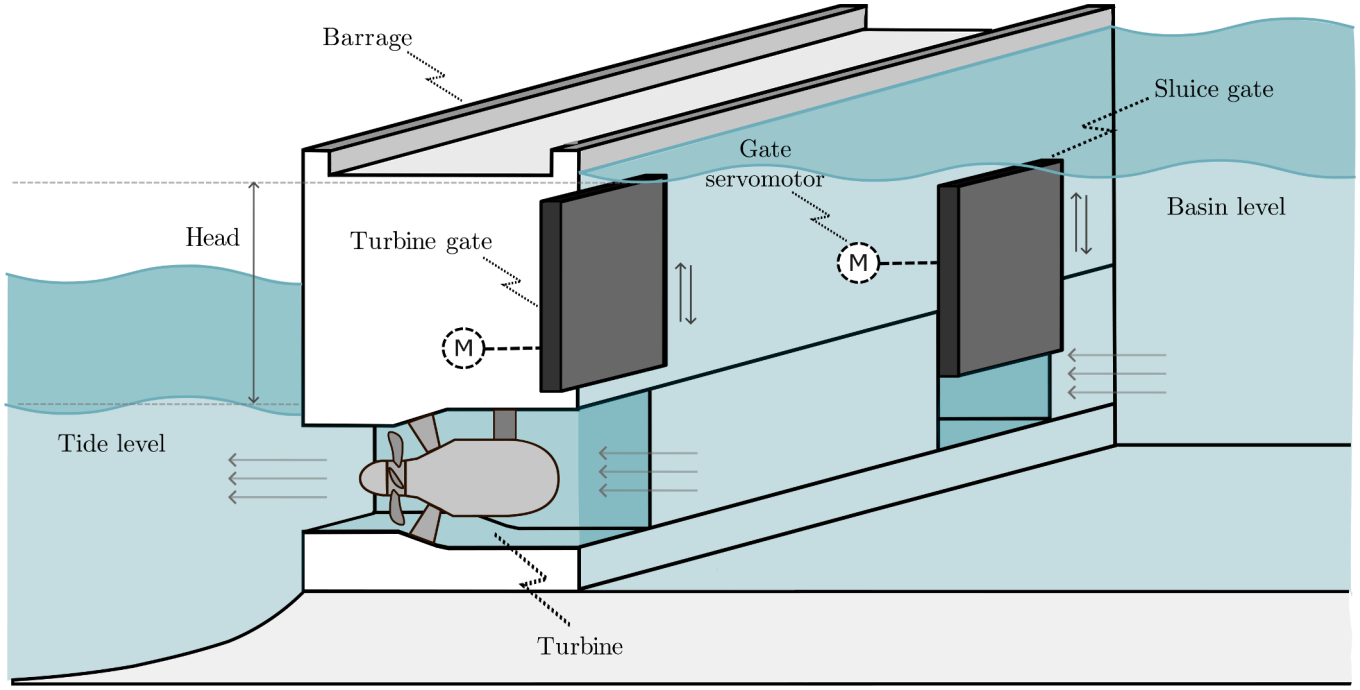

Fig. 1. Schematic representation of a tidal barrage.

$$F_g = \frac{gMm}{d^2}, \tag{1}$$

where F_g is the gravitational force between M (the mass of the Moon or Sun) and m (the mass of a molecule of water located in the sea), d is the distance between both masses, and g is the universal constant of gravitation.

The gravitational interaction between the three celestial bodies can be explained by first considering the gravitational force exerted by the Moon. Because the Earth is not a point mass, each molecule on Earth is subject to a different gravitational force; the solid material of the Earth experiences only a small deformation due to the gravitational force from the Moon, but the water on the Earth's surface is free to move. A molecule of water located on the Earth's side that is facing the Moon will undergo a greater gravitational force than the rest of the mass on Earth, since its distance from the Moon is the shortest. On the other hand, when a molecule of water is on the opposite side of the Earth, the distance to the Moon is the greatest, and the gravitational force is less than on the rest of the mass on Earth. In both cases, there is a separation between the molecule of water and the solid mass on Earth, which translates into a rise in sea water level. The result is a tidal height variation with two peaks per lunar day (a lunar day lasts 24 h and 50 min). The same interaction is seen with the Sun, but because the Moon is relatively closer to the Earth, its gravitational force is 2.17 times higher than that of the Sun [20], despite a mass ratio of the Sun to the Moon of 27×10^6. Spring (peak) tides occur when the Sun and Moon are lined up with the Earth (new Moon and full Moon), and neap (low) tides occur when they form a 90-degree angle with the Earth. Fig. 2 shows a representation of the gravitational interaction between the Earth, Moon and Sun that generates spring and neap tides.

Moreover, the gravitational force between the Earth and the Moon is balanced by a centrifugal force that maintains the distance d constant:

$$F_c = ml\omega^2, \tag{2}$$

where F_c is the centrifugal force on m, l is the distance between the molecule of water and the centre of revolution between Earth and Moon, and ω is the angular velocity of the Moon with respect to the Earth. Because the Earth has 80 times more mass than the Moon, the centre of revolution O_c is located 'inside' the Earth, as seen in Fig. 3. As a result, each element of mass on Earth is not at equilibrium with respect to the Moon, and so the centrifugal force tends to push the water outward from the Earth, further increasing the sea water level.

The gravitational and centrifugal forces alone do not explain the tidal levels that can be found in near-shore areas. The hydrodynamics of the tides, determined by the length, width and depth of the shore in a specific site, are responsible for the tidal amplitude and phase, and for the speed and timing of tidal currents. The local enhancement of tides in

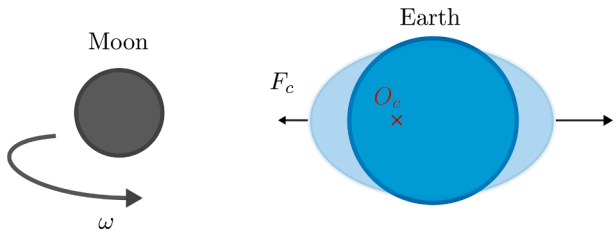

Fig. 3. Centrifugal force balancing the gravitational force between the Moon and the Earth.

estuaries or bays is mostly due to resonance coupling to natural frequencies of water movement, somewhat similar to the way woodwind instruments resonate. The incident tides are subject to shoaling (decrease in water level when approaching shallower regions) and reflection, which can cause constructive interference [21]. These phenomena take place in certain places across the globe and make the tidal resource highly site-specific.

The tidal level n_o can be represented as the sum of different harmonic constituents, as described in Eq. (3). Each constituent i has a certain period T_i, corresponding to a frequency ω_i, that depends on the particular phenomenon that causes each specific constituent, and a certain amplitude A_i (in meters) and phase ϕ_i that depend on the location of the tidal height measurement point on Earth:

$$n_o(t) = \sum_{i=1}^{N_i} A_i \cos(\omega_i t - \phi_i). \tag{3}$$

where N_i is the number of constituents considered. The resulting total variation is that of a modulated sinusoid with variable amplitude, caused by constructive and destructive interference between constituents.

Table 1 lists the most relevant semidiurnal and diurnal tidal constituents. The semidiurnal constituents, identified with the subscript 2, have two peaks per day, and the diurnal constituents, identified by the subscript 1, have one peak per day. The Cartwright potential coefficient is a dimensionless measure of the expected relative amplitude of the tidal constituents [22]. At most sites, the two constituents with the highest amplitude are the lunar semidiurnal M_2 component (caused by the gravitational interaction between Earth and Moon) and solar semidiurnal S_2 component (caused by the gravitational interaction between Earth and Sun). However, the amplitude of each constituent varies in each location on Earth: at some sites, the diurnal constituents are more prominent than the semidiurnal ones, leading to only one high tide per day. Other constituents are produced by several asymmetries such as the orbits of the Moon and Sun, which are elliptical rather than circular, and the tilt of the equatorial plane with respect to the Earth's orbit plane.

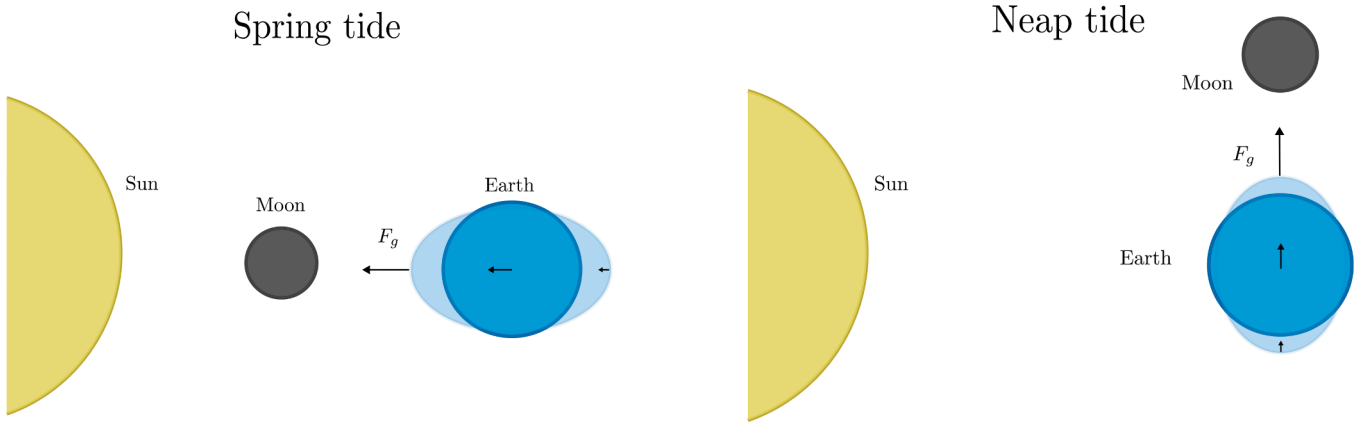

Fig. 2. Spring and neap tides generated by the gravitational force F_g between the Earth and Moon, and the Earth and Sun.

Table 1
Main semidiurnal and diurnal tide constituents, their period in hours and Cartwright potential coefficient (expected relative amplitude of the tidal constituents) [22].

Type	Symbol	Description	Period [h]	Cartwright potential coefficient
Semidiurnal	M_2	Principal lunar	12.421	0.9081
	S_2	Principal solar	12.000	0.4299
	K_2^L	Declinational to M_2	11.967	0.0768
	K_2^S	Declinational to S_2	11.967	0.0365
	N_2	Elliptical to M_2	12.658	0.1739
	L_2	Elliptical to M_2	12.192	0.0257
Diurnal	O_1	Principal lunar	25.819	0.3769
	P_1	Principal solar	24.066	0.1755
	K_1^L	Declinational to O_1	23.934	0.3623
	K_1^S	Declinational to P_1	23.934	0.1682
	Q_1	Elliptical to O_1	26.868	0.0722

Tides are also influenced by local weather conditions, such as wind speed and direction, atmospheric pressure, or water density (due to temperature and salinity variations). In particular, water level variations associated with wind and atmospheric pressure are known as 'storm surges'. Unlike the fundamental periodic astronomic interactions that originate the tides, these stochastic weather-driven factors are relatively unpredictable. However, their influence is relatively small compared to the fundamental periodic behaviour of the tides.

2.2. Global tidal range resource

The annual theoretical energy per squared meter that can be extracted from the tidal range resource is calculated with the following formula [14]:

$$\mathrm{PE} = \sum_{i=1}^{N} \frac{1}{2} \rho g H_i^2, \tag{4}$$

where ρ is the water density, H_i is the peak water elevation with respect to the mean seawater level for each i successive rising and falling tide, and N is the number of rising and falling tides in a year ($N \simeq 1411$). Table 2 shows those countries with the highest annual potential energy due to water level variations, calculated with this formula, and using five tidal constituents as given in [14]. This analysis assumes that the acceptable areas where the tidal range resource can be exploited are those where the water depth is less than 30 m and the annual energy yield is greater than 50 kWh/m^2. Note that, for tidal range schemes, the location is generally restricted to relatively shallow waters with a maximum water depth of $\sim$ 30 m, in order to assure the feasibility of the project [21].

Table 2
Annual energy yield per country [14]

Country	Annual potential energy [TWh]	Percentage of global resource
Australia	1760	30%
Canada (Fundy)	1357	23%
UK	734	13%
France	732	13%
US (partial sea ice)	619	11%
Brazil	298	5%
South Korea	107	2%
Russia (partial sea ice)	75	1.3%
Argentina	62	1.1%
India	19	<1%
China	12	<1%

As a reference, the global electricity demand in 2020 was $\simeq$ 25000 TWh [23], meaning that the theoretical potential of the tidal range is more than 20% of the global electricity consumption. It can be seen from Table 2 that 90% of the tidal range resource is located across only five countries. However, these areas might also present limitations for tidal barrage developments due to environmental, social or economic constraints, lowering the actual available energy for electricity production.

3. Tidal barrage power plants

This section focuses on the operating modes of tidal power plants, the different configurations of tidal range schemes, and their environmental impact. Furthermore, the current tidal barrage plants in operation are listed, including proposed projects.

3.1. Types of tidal range power plants

Tidal barrage power plants can be categorised, in terms of design, into three groups: Single-basin barrages, linked-basin barrages and tidal lagoons. In single-basin barrages, an embankment is constructed to separate the estuary from the open sea, thus creating an artificial reservoir (Fig. 4a). The water flows in and out of the reservoir through turbines and sluice gates located across the embankment. The generation periods alternate with sluicing and holding periods depending on the tidal water level in the open sea, and so the power output is not continuous throughout the day.

Linked-basin barrages (Fig. 4b), on the other hand, are conceived with the purpose of supplying continuous power, with an overall decrease in energy generation compared to single-basin schemes, but with the advantage of better matching energy supply to demand. They consist of two basins (a high water basin and a low water basin) that are internally connected through turbines, and each is separately connected to the open sea through sluice gates, as seen in Fig. 4b. Hence, there are three different operational heads: Between the sea and the high water basin ($H_{HW,o}$), between the sea and the low water basin ($H_{LW,o}$) and between basins ($H_{HW,LW}$). The high water basin is filled when the tide rises so as to keep the water level inside of it n_{HW} as high as possible at all times (hence the name 'high water basin'). The low water basin is emptied when the tide decreases to keep the water level inside of it n_{LW} as low as possible. As a result, a sufficient head $H_{HW,LW}$ is maintained between basins, which is used to generate electricity. The downside of linked-basin schemes is that the investment cost is even higher than that of single-basin barrages, with considerably lower energy output. The study in [21] shows that the energy output of a linked-basin scheme is less than 43% of the generated energy from an equivalent single-basin scheme.

Another type of tidal range plant is the tidal lagoon, which is a particular configuration of a tidal barrage. Tidal lagoons are schemes located on a shore, and the embankment has a semi-circular shape that encloses the basin. They can also be completely off-shore schemes, where the embankment alone encloses the complete basin. Fig. 4c shows a representation of a tidal lagoon. It can be seen that the embankment is much larger in a lagoon scheme than in the case of tidal barrages. Therefore, tidal lagoons may require a higher civil cost, but with the advantage that they can be located in a wider range of sites.

3.2. Modes of operation

There are three modes of operation for tidal barrages: generating on ebb, generating on flood, and two-way generation. Fig. 5 shows a schematic representation of the three modes.

Ebb generation (Fig. 5a) means that the turbines operate when the water level inside the basin is higher than the sea level. As the tide level increases, the basin is filled through sluice gates until the basin water

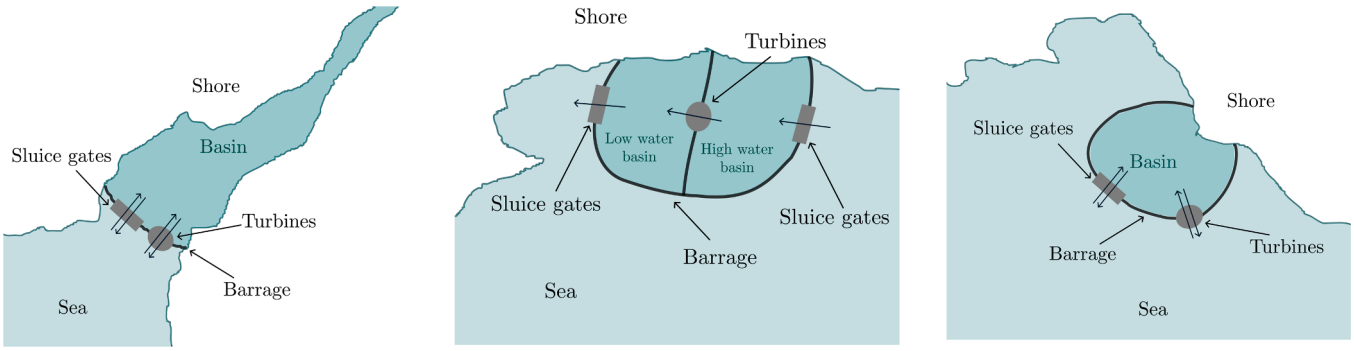

(a) Single-basin barrage scheme. (b) Linked-basin barrage scheme. (c) Tidal lagoon scheme.

Fig. 4. Schematic representation of tidal barrages and tidal lagoons.

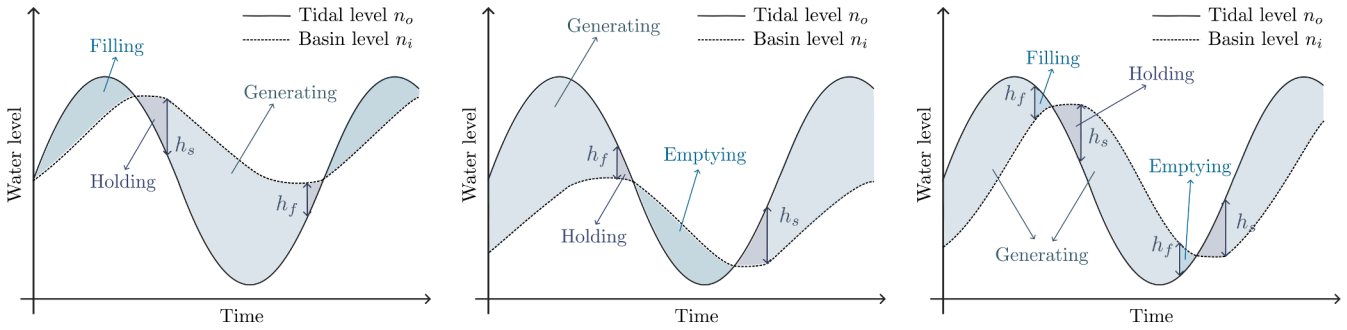

(a) Ebb generation mode (b) Flood generation mode (c) Two-way generation mode

Fig. 5. Types of tidal barrage operating modes for energy generation (excluding pumping).

level matches the sea level. The sluice gates are then closed to hold the water level while the sea level decreases, until an appropriate head (starting head, denoted in Fig. 5 by h_s) is created. At this point, the basin is emptied through the turbines, and the potential energy given by the aforementioned head is transformed into mechanical energy. Generation stops when a minimum head (finishing head, denoted in Fig. 5 by h_f) is reached, and the inner water level is held until the tide level starts to increase again, and the cycle repeats.

On the other hand, flood generation (Fig. 5b) means that the basin is filled through the turbines and emptied through the sluice gates. When the sea level rises, and a high enough head is created between the sea and the water inside the basin, the turbines start operating while filling the basin. After the generating phase finishes and the sea level starts decreasing, the basin is emptied through sluice gates, and the cycle repeats. In general, flood generation is less efficient than ebb generation because of the topology of the basin: the surface of the basin tends to be greater at the top, so there is more volume of water contained in the upper half of the basin (where ebb generation operates) than in the lower half (where flood generation operates) [24].

Two-way generation (Fig. 5c) combines ebb and flood generation to distribute the energy production more evenly throughout the day, but with a consequent decrease in maximum instantaneous power output. This mode of operation requires the use of reversible bulb turbines that can generate electricity for bidirectional water flow. Bidirectional operation also requires longer water passages and therefore higher investment costs [25].

The turbines can also be used as pumps in order to increase the instantaneous operating head. When the basin level is equal to the sea level, energy is consumed by the pump to further fill or empty the basin so that the available head during the following generation phase is higher. Given the periodic nature of the excitation force (*i.e.* the tide level), the result is that, by injecting this additional energy into the system, the overall net energy production of the cycle increases. The increase in net energy gain can be up to 13% of the energy generation without pumping, as seen in [26].

In the case of linked-basin barrages, the flow through the structures is directed in only one way, as seen in Fig. 4b. Therefore, the turbines are not reversible, and operate at a relatively constant head. The operation of linked-basin schemes is shown in Fig. 6.

3.3. Environmental and social aspects

One of the major challenges for the development of tidal barrage power plants is their environmental impact. The construction of the embankments alters the natural water flow in the site, affecting the

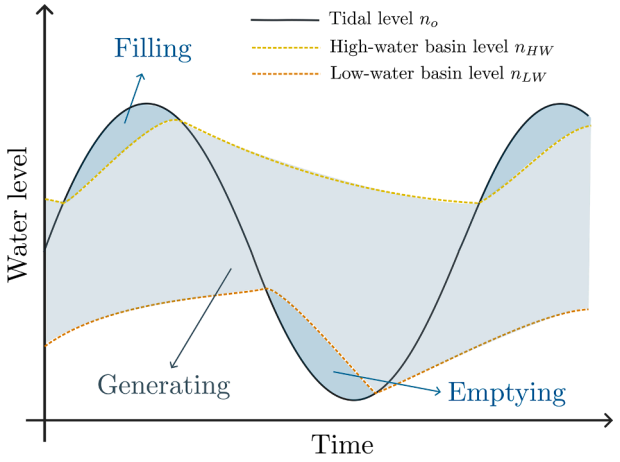

Fig. 6. Operation of a linked-basin barrage, where n_o is the sea water level (bold line), n_{HW} is the water level in the high water basin and n_{LW} is the water level in the low water basin.

wetted lands, sediment transport, marine life, and navigation. It also affects the tidal range of the site because the structures of the barrage can cancel or enhance particular resonance modes of the estuary.

The environmental impact of the barrage may vary with the chosen operational mode, *i.e.* one-way or two-way generation. In one-way generation, the basin range (the difference in height between the maximum and minimum basin water level) may decrease compared to the tidal range, and the mean water level inside the basin may either increase (in case of ebb generation) or decrease (in case of flood generation), compared to the mean sea water level. The change in mean water level inside the basin has an impact on the wetting and drying processes on the shore, affecting the local flora and fauna. For instance, increasing the mean water level may permanently submerge mud flats and reduce salt marsh areas. On the other hand, operating in two-way generation could reduce the impact on the basin range and maintain the mean water level inside the basin closer to the mean sea water level. [25] studies the hydro-environmental impact of different operating modes in the Severn Estuary, where, in two-way generation, restricting the holding period results in lower energy output but also reduces the change in basin range and the inter-tidal area loss.

In tidal barrages, the embankment completely blocks the stream or estuary where the basin is located and, therefore, the barrage has a considerable impact on the environment, as well as on navigation. To mitigate this impact, ship locks and passageways for fish are added to the embankment. Tidal lagoons, on the other hand, have the same principle of operation as barrages but the dam structure is located in a shore, instead of blocking an estuary. This avoids interfering with fish migration and navigation channels, and allows the development of tidal range projects in less environmentally sensitive locations [25].

By blocking the natural water flow, the barrage decreases the velocity of the tidal currents, which could potentially have a positive impact on biodiversity. The study in [27] shows that the reduction of tidal current velocities in the Severn Estuary can reduce the level of suspended sediments inside the basin and turbidity levels, which increases the light penetration in the water column and could potentially increase biodiversity at the site. Another positive side of tidal barrages is that they can provide road links between shores and increase the economic activity and tourism of the area, as seen, for instance, in the case of the La Rance power plant [21].

Tidal schemes can also be used for flood prevention in nearshore areas, which will become increasingly critical with sea level rise due to climate change and ice melt from the poles. Sea level rise is likely to affect tidal dynamics, ocean water density, tidal amplitudes and period, sediment transport and biogeochemical systems, but there is a high level of uncertainty as to how the available resource will change [28]. If a tidal plant is constructed with the additional purpose of flood prevention, special design considerations must be taken into account. For instance, the height of the embankment should be designed for 150-year storm surges [29].

3.4. Tidal barrage plants in operation

Given that the tidal resource is site-specific and can be harnessed in a few locations around the world, only a small number of countries have developed tidal projects. Many publications on tidal energy operation consider these existing plants as case studies to compare and validate their results.

3.4.1. La Rance (France, 1966)

The first tidal barrage project to be built and start operating was the La Rance power plant, located in Brittany, France. It consists of a 720 m embankment and a basin area of 22 km^2, with 24 10 MW bulb turbines and six sluice gates, resulting in an installed capacity of 240 MW and an annual energy output of around 480 GWh. The turbines are reversible, therefore the plant operation is two-way generation with pumping. The tidal range resource in the site is between 9 m and 14 m. The barrage itself acts as a four-lane highway, which has shortened the travel between the towns of Dinard and St Malo by several hours [3].

As the first of its kind, the La Rance plant required major civil works, including the removal of 1,500,000 m^3 of water and the drying up of 75 hectares of the estuary [3]. This was avoided in later projects with the use of submersible caissons instead of cofferdams, thus preventing such a high impact on the site [21]. The barrage provides a pathway for fish in order to preserve the local species, and the fishing industry has remained unaffected, although one species, the lanson, has disappeared. In spite of these environmental issues, the plant is generally regarded as a success for its reliability and positive impact on transportation and tourism [21].

3.4.2. Sihwa Lake Tidal Power Station (South Korea, 2011)

Sihwa Lake tidal power plant, located in the Gyeonggi Province, is currently the largest tidal barrage scheme in operation, with 254 MW of installed capacity. The plant generates on flood only, which helps maintain a low water level inside the basin and prevent flooding of the already existing infrastructure nearby. The mean spring tide range is 7.8 m and the basin surface area is 42.4 km^2.

The embankment was originally constructed in 1994 for flood mitigation and agricultural purposes [4], but the closed nature of the basin meant that it was prone to waste accumulation due to the industrial developments nearby. To provide the passage of freshwater and improve circulation, the dam was reengineered by adding 10 25.4 MW bulb turbines, turning it into a tidal power plant.

3.4.3. Jiangxia Experimental Tidal Power Plant (China, 1980)

The Jiangxia Experimental TPP is located in the Wenling County, Zhejiang Province, where the tidal range has a mean of 5.08 m and a maximum of 8.39 m. The area of the basin is $\sim$ 1.5 km^2 and is contained by a clay-core rockfill embankment of 670 m in length. The plant started operating in 1980 with one bi-directional 500 kW bulb turbine. After three decades of expansion and technological upgrading, the plant has now 6 turbines and a total installed capacity of 4.1 MW, making it the largest operating tidal plant in China [30]. The 6 turbines are reversible, allowing the operation to be two-way, with pumping.

3.4.4. Kislaya Guba (Russia, 1968)

Kislaya Guba was built in 1968 with an installed capacity of 400 kW, and was later expanded to 1.7 MW [14]. The turbines are of bulb type, the embankment is only 40 m wide, and the impounded basin area is 1.1 km^2. It is located in a fjord near Murmansk, in the Kola Peninsula, where the tidal amplitude is 2.5 m and it is the only tidal plant located in the Arctic. The scheme stands out because it was built entirely by women engineers [31].

3.4.5. Haishan Tidal Power Plant (China, 1975)

The Haishan TPP is the only operational linked-basin tidal scheme in the world. It was built in 1975 and, together with Jiangxia TPP, is the only tidal plant in China still in operation. It is located in Yueqing Bay, in the Zhejiang Province, where the tidal range is 4.87 m.

This double basin plant has the advantage, as outlined in Section 3.1, of being able to generate electricity almost constantly. The installed capacity is 150 kW, and pumping was added later on to add storage capacity and enhance the stability of the power supply to the grid. The plant can generate from 27 to 30 days per month and 20.5 h to 22.1 h per day [30].

3.4.6. Annapolis Royal Generating Station (Canada, 1984–2019)

The Annapolis Royal Generating Station was located on the Annapolis River in the Bay of Fundy, Nova Scotia, where the tidal resource is the second highest in the world (see Table 2). It had a single 20 MW Straflo turbine which operated on ebb generation. The plant was decommissioned in 2019 due to the high fish mortality that was associated with turbine operation [18].

3.5. Proposed projects

Several locations worldwide have been considered in the literature as potential sites for tidal barrage schemes, such as Western Australia [32], the Zhejiang Province in China [30], the Patagonian Shelf in Argentina [33], the Bacanga Estuary in Brazil [34], and the Gulf of California in Mexico [35]. A location that stands out for being studied the most is the Severn Barrage and Bristol Channel in the United Kingdom, where several projects were proposed throughout the years.

The coast of the UK has the third highest tidal range resource in the world (see Table 2). The theoretically available energy from the UK tidal range is more than double its electricity consumption, which was just below 300 TWh in 2022 [36]. The UK government had a target of a 80% reduction of greenhouse gas emissions by 2050, and it was recently lowered to a net-zero emissions target [37], which calls for an extensive use of renewable sources, including tidal range energy. Several sites are currently being considered around the coast of the UK. [38] reports a detailed study of the tidal energy potential that can be exploited on the coast of the Eastern Irish Sea, including hydrological, morphological and environmental impacts. The literature on tidal barrages has used sites on this coast as study cases, such as Solway Firth [6], Morecambe Bay [29] and Mersey Estuary [39], as well as the North Wales coast [40].

The most discussed locations for tidal range energy in the UK are the Seven Estuary and Bristol Channel. The Severn Estuary and Bristol Channel are located in the Southwest of the UK, where the peak tidal range is 14 m. The literature contains studies using parameters from possible schemes at this site, such as the Severn Barrage [41], Fleming Lagoon [27], Cardiff-Weston Barrage [2], West Somerset Lagoon [42] and Swansea Bay Lagoon [43]. [25] studies the hydrodynamic interaction between several proposed projects in the Severn Estuary and Bristol Channel. In particular, the 'Hendry Review' [44] highlights the importance of tidal lagoons in decarbonising the UK electrical grid in a cost-effective way and, in particular, gives recommendations for the development of the Swansea Bay Tidal Lagoon project. However, there is still no consensus on the economic feasibility of these proposed projects and their environmental impact, including the impact on fish and bird populations [45].

4. Modelling of tidal barrages

This section presents an account of the different modelling approaches that can be found in the general literature on tidal barrage design and operation, with an emphasis on the models employed for control and optimisation purposes. The models will determine the dynamics of the representation associated with the tidal range structures, as described later on in Section 5, which underpins the importance of model selection for tidal barrage control. In general, tidal barrage models include the following subsystems, using the same terminology as in Eq. (20):

n_o: The tidal range temporal variation,

$\mathscr{H}$: the near and far-field hydrodynamic processes inside and outside the basin,

$\mathscr{B}$: the topology of the basin,

$\mathscr{T}$: the hydraulic turbine characteristics,

$\mathscr{S}$: the sluice gates, and

$\mathscr{E}$: the electrical coupling with the power grid.

Fig. 7 shows the time scales corresponding to the dynamic behaviour of some of these subsystems. It can be seen that the time scale at which the tide elevation varies is several orders of magnitude larger than that of the other subsystems. As a result, the operation of a barrage can be modelled by considering these subsystems to be in a quasi-steady state with respect to the tidal level variations, without a significant loss of accuracy. However, special consideration should be given to hydrodynamic modelling: the construction and operation of the barrage affect both the mean water level inside the basin, and the tidal current speed outside the basin [28], thus having an impact on the tidal level variations.

Tidal barrage models are necessary to assess the power production of a tidal barrage scheme, as well as its impact on the surrounding environment, and to perform operational optimisation studies. As will be described in the remainder of this section, tidal barrage models typically include several nonlinear elements: The hydrodynamic processes (except in the 0D model), the turbines, and the sluice gates. Nonlinearity is a key attribute of tidal barrage models that has to be considered for the selection of optimisation strategies and solvers. The study in [46], on the other hand, uses a linearised model of a tidal lagoon in order to implement a Mixed-Integer Linear Programming (MILP) formulation, to reduce the computational complexity of the problem. Although this approach could be useful for a first assessment of the possible energy output of a tidal barrage, a linearised model may compromise the optimality of the solution when implemented for optimal control purposes.

Tidal barrage modelling in the literature focuses mostly on mathematical and physical models computed by leveraging first principles, though data-driven models have been considered in the case of the turbines, which are provided *a priori* by the manufacturer. Models derived from experimental data, very much in the spirit of system identification [47], can potentially give a simplified (yet representative) mathematical description of the subsystems that form a tidal barrage plant, but such models are uncommon in the literature, given the small number of operating tidal barrage plants currently active in the world. To the best of the authors' knowledge, only [48] presents a data-driven

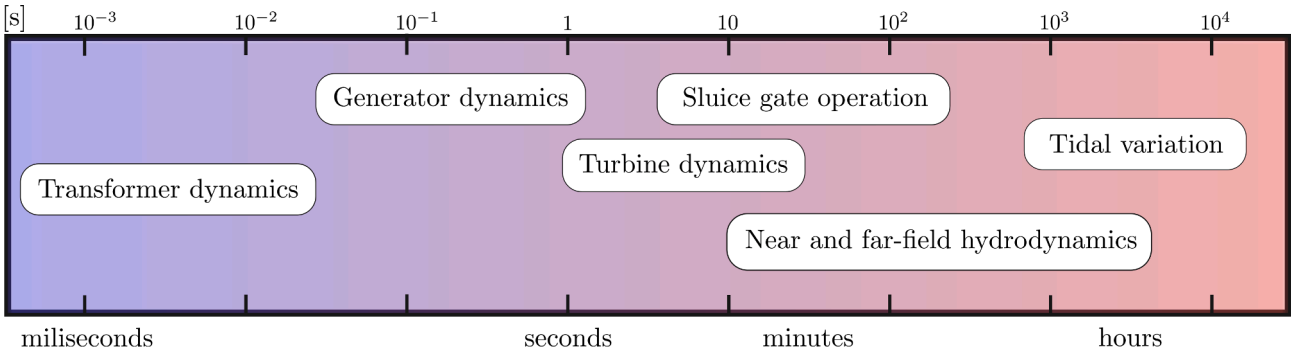

Fig. 7. Time scales of the different subsystems of the tidal barrage model.

artificial intelligence (AI) model of the La Rance tidal barrage, where data from the operation of the power plant is used to parameterise the turbine, sluice gate, and basin models. However, data-driven models have not been yet implemented for hydrodynamic modelling of tidal barrages, which is indeed a significantly complex and computationally demanding feature of any representative tidal barrage dynamic model.

4.1. Tidal level variation

As previously discussed in Section 2.1, the tide can be modelled as the sum of different tidal constituents. Which constituents to include in the model is commonly decided depending on the selected site. Fig. 2.1 shows an example of a tide modelled using four constituents: M_2, S_2, O_1 and $K_1 = K_1^L + K_1^S$, parameterised according to Table 1. These four constituents are the most prominent ones in most sites; several studies in the literature use only these to model the tidal elevation, with different amplitudes depending on the specific location under analysis, as seen for instance in [49]. It is also a common practice to use either the eight tidal constituents $M_2, S_2, N_2, K_1, Q_1, O_1, P_1$ and K_2 [43], or ten constituents (by adding S_1 and M_4) [25]. The constituents for a particular site can be found in high-resolution global tidal databases such as TPXO [50] or MIKE21 [51].

The number of constituents included also depends on the time span of the simulation. For instance, if the simulation is done for a time window of two days, the tidal variation will not show the spring-neap cycle, as seen in Fig. 8; therefore, S_2 could be removed from the model. A criterion for choosing the constituents based on the time span of the simulation is to calculate the synodic period between constituents. In particular, the synodic period T_{syn} is the time required to separate the effect of two tidal constituents, and can be calculated using Rayleigh's criterion [22]:

$$T_{syn} = \frac{1}{|f_1 - f_2|}, \tag{5}$$

where f_1 and f_2 are the frequencies of each constituent. Naturally, each constituent has a certain energy contribution (in terms of seawater elevation) that should be accounted for whether the constituent is modelled or not. That is to say that the constituents that are indeed modelled should be scaled in order to include the energy contribution of those constituents which are not modelled.

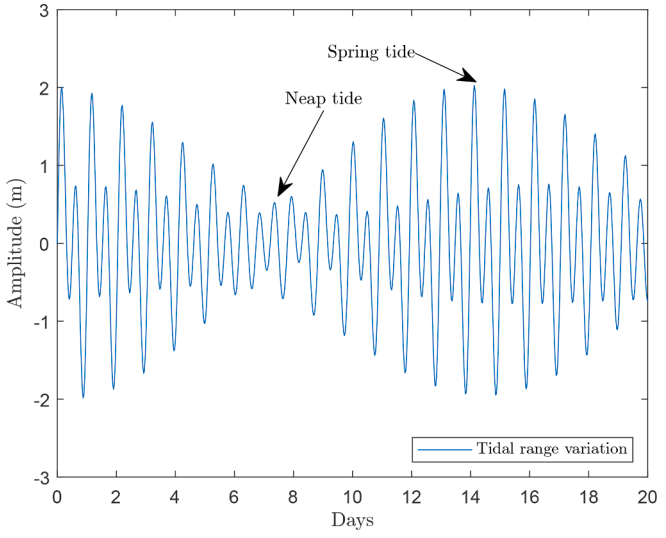

Fig. 8. Example of a tidal range variation modelled as the sum of the four constituents M_2, S_2, O_1 and $K_1 = K_1^L + K_1^S$.

4.2. Hydrodynamic modelling

The hydrodynamic domain of interest consists of an open sea subdomain and an upstream (inner basin) subdomain, both linked by the hydraulic structures of the embankment, *i.e.* turbines and sluice gates. The hydrodynamic processes in these subdomains can be described using four different approaches, namely 0D, 1D, 2D and 3D models, with an increasing fidelity. The simplest model is 0D, where the hydrodynamics of the water flow are not considered, and the open sea level is predefined, while the higher dimensional (1D, 2D and 3D) models take into account (with different levels of accuracy) the impact of the barrage on the local and regional hydrodynamics, to predict the tidal range in the vicinity of the embankment. Fig. 9 shows a schematic representation of the parameterisation involved in 0D, 1D and 2D models.

The tidal level is described in terms of individual tidal constituents, as discussed in Section 4.1. In 1D, 2D and 3D models, the tide is used as a boundary condition to calculate the water elevation throughout the open sea subdomain. On the other hand, in 0D models, the water level is considered constant in space and the water elevation immediately next to the barrage is assumed to be equal to the tidal level.

For ease of computation, 0D models are usually used to perform the

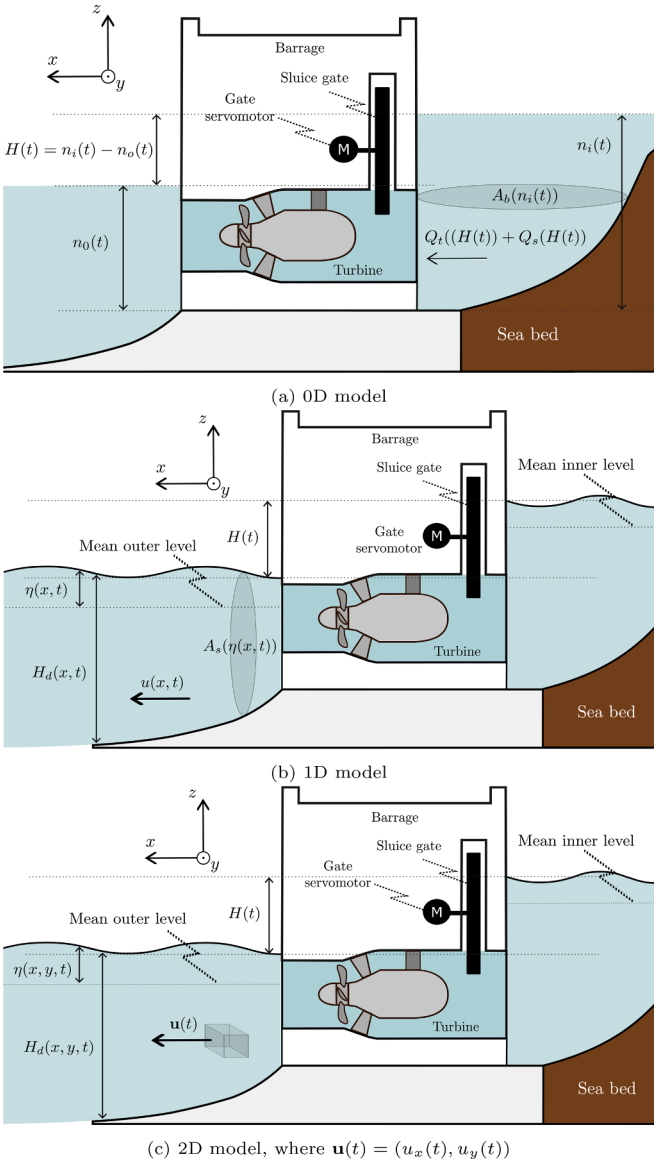

Fig. 9. Representation of the parameters of the 0D, 1D and 2D models.

optimisation of tidal barrage operation. Then, the resulting operation is applied to the 2D model to simulate the performance of the plant and validate the results from the 0D model, as seen for instance in [52]. It is clear that the water elevation in the vicinity of the barrage, calculated by the 2D model, is different than that computed with the 0D model (*i.e.* the tidal elevation without a barrage). Therefore, the operation is not optimised for the tidal elevation that the site would actually have if the barrage was in place. This issue is dealt with in [7]: The optimised operational protocol obtained with the 0D model is applied to the 2D model simulation, and the resulting tidal elevation from the 2D model is then used in a second iteration to refine the corresponding barrage operation. The results show almost no change in energy generation between the solution from the first optimisation and the solution from the second iteration, although this might vary in different schemes, and with different operating modes. Note that the study in [7] considers small-scale schemes, which have a low impact on the local hydrodynamic processes; for larger barrages, the 0D model might not be sufficient, and higher-dimensional models, which effectively consider the momentum equation, can become important.1D, 2D and 3D models are also necessary to analyse the environmental aspects associated with the barrage, such as variations in the wetting and drying processes on the shores, sediment transport, water quality, and biological processes. A number of hydro-environmental models have been developed to analyse physical, chemical and biological conditions in coastal and estuarine areas [53]. These models can be particularly useful to accurately quantify the environmental impact of tidal barrage operation. For instance, [54] presents a hydro-environmental 2D model that describes solute transport and the interaction between bacteria and sediments in water. Furthermore, [55] proposes a species distribution model that, coupled with a 2D model, is considered in the Severn Estuary to examine the impact of a proposed barrage scheme on the fauna of the site. Note that, in [54], simplified operation of a barrage is considered, so a further natural step would be to consider the hydro-environmental model together with a more accurate tidal barrage description, or even directly use a hydro-environmental model, when optimising the tidal barrage operation.

Clearly, the high computational burden associated with 1D, 2D and 3D models is a challenging aspect of tidal barrage modelling. Reducing the complexity of these models, while preserving an accurate description of the hydrodynamic processes that effectively take place in a tidal barrage, can potentially enable their use in optimal control design (and, in general, optimisation) of tidal barrages. A way of achieving this would be to use measured data to parameterise simpler hydrodynamic models, as mentioned at the beginning of Section 4, although this can only be applied to the study of existing tidal barrage plants where operational data exists. An alternative is to use data generated from 1D, 2D and 3D high-fidelity models, instead of measured data, to parameterise simpler models. Lessons can be learned from the wave energy field, where hydrodynamic system identification has been studied by using both high fidelity models [56] and measured data [57],while also techniques from the field of model reduction can be effectively useful to produce parsimonious descriptions (see e.g. [58]).

4.2.1. 0D models

The 0D, or flat-estuary, model assumes that the water level is constant throughout the basin and the sea, and does not account for the water velocity distribution along each subdomain under study. To compute the instantaneous head, only the total water flow through the embankment is considered, without taking into account the spatial distribution of the sluice gates and turbines. The change in water level inside the basin is calculated by the principle of mass conservation, *i.e.*

$$\frac{\mathrm{d}n_i}{\mathrm{d}t} = \frac{Q_t + Q_s}{A_b(n_i)}, \tag{6}$$

where $n_i(t)$ is the inner basin water level, $H(t) = n_i(t) - n_o(t)$ is the head computed as the difference between the inner basin level $n_i(t)$ and the outer sea level $n_o(t)$, $Q_t(H(t))$ and $Q_s(H(t))$ are the turbine and sluice gate flows, respectively, and $A_b(n_i(t))$ is the wetted surface area impounded by the basin.0D modelling requires less computational resources than the 1D, 2D and 3D counterparts, and can give a reasonable approximation of the overall energy yield. Therefore, the 0D model is effectively common in the literature for resource assessment [6], fixed parameter optimisation [59] and optimal control [11] of tidal range energy. The downside of the 0D model is that it does not take into account the impact of the barrage and its operation on the tides, which means that the power production estimates are usually overoptimistic [52].

4.2.2. 1D models

The one-dimensional (1D) model assumes that the flow can be integrated both in the vertical dimension and across the width of the basin. As a result, the water velocity has only one component, *i.e.* is a scalar value. The interaction of the barrage with the regional hydrodynamics is modelled using the one-dimensional shallow water equations, also known as the Saint–Venant equations [60]:

$$\begin{aligned} \frac{\partial A_s}{\partial t} + \frac{\partial (A_s u)}{\partial x} &= 0, \\ \frac{\partial u}{\partial t} + u\frac{\partial u}{\partial x} + g\frac{\partial \eta}{\partial x} &= -\frac{\tau_b}{\rho H_d}, \end{aligned} \tag{7}$$

where $\eta(x,t)$ is the free surface elevation, $A_s(\eta(x,t))$ is the cross-sectional area of the water, $u(x,t)$ is the depth-average velocity (orthogonal to $A_s(\eta(x,t))$), $H_d(x,t)$ is the total water depth, and τ_b is the bed shear stress along the perimeter of the cross-sectional area $A_s(\eta(x,t))$. Note that the equations are solved both in the open sea subdomain and inner basin subdomain. Each subdomain is discretised by a certain number of cross-sections (of area A_s) parallel to the barrage and orthogonal to the water flow. The water elevation is calculated on each cross-section, and the hydraulic head that determines the flow through the structures (turbines and sluice gates) is the difference between the water elevation from the cross-sections on either side of the barrage.

The 1D model can be useful for small-scale tidal schemes or for optimisation purposes, due to their computational efficiency [60]. There are some examples of the application of 1D models in the tidal energy literature, although it is significantly less common than the use of 0D and 2D models: [61] studies the available power of a tidal barrage in the Bristol Channel, while [62] analyses the optimum position of a barrage in the Severn Estuary. In particular, [63] presents a novel numerical technique for 1D modelling, alternative to the explicit finite difference-based numerical methods, known as Incremental Differential Quadrature Method (IDQM). The study shows that IDQM has unconstrained stability, meaning that the time step can be relatively large, allowing long timescale simulations. IDQM also allows the use of a lower number of grid points without loss of accuracy, which could enable its efficient application in tidal barrage optimisation.

4.2.3. 2D models

The appeal of the 2D model is that it allows for fairly accurate results with reasonably manageable computational requirements for simulation purposes. In this case, the depth-integrated water velocity is assumed horizontal, with both longitudinal (x) and lateral (y) components. The governing equations are the 2D shallow water equations, which can be written in non-conservative form [7] as

$$\begin{aligned} \frac{\partial \eta}{\partial t} + \nabla\cdot(H_d\mathbf{u}) &= 0, \\ \frac{\partial \mathbf{u}}{\partial t} + \mathbf{u}\cdot\nabla\mathbf{u} - \nu\nabla^2\mathbf{u} + f_C\mathbf{u}^{\perp} + g\nabla\eta &= -\frac{\tau_b}{\rho H_d}, \end{aligned} \tag{8}$$

where $\mathbf{u}(t) = (u_x(t), u_y(t))$ is the water velocity vector, ν is the kinematic viscosity of the fluid, and f_C is the Coriolis acceleration defined by $f_C = 2\omega_e \sin\phi$ with ω_e the angular frequency of the Earth's rotation (in rad/s),

$\mathbf{u}^{\perp}$ is the velocity vector rotated 90° counter-clockwise, and ϕ the latitude. It can be seen from (8) that the parameterisation of the model is more complex due to the added viscosity and Coriolis terms ($\nu\nabla^2\mathbf{u}$ and $f_C\mathbf{u}^{\perp}$, respectively). The equations in (8) are solved numerically by dividing each subdomain (*i.e.* open sea and basin) into cells, forming an unstructured mesh. The resolution of the mesh is usually low closer to the boundaries, with an order of magnitude of some kilometres, increasing when closer to the embankment, where it can reach tens of meters. The hydraulic head that determines the flow through the turbines and sluice gates is calculated as the difference between the water elevation in the nodes of the cells on each side of the barrage. Several 2D ocean computational models are used in the literature to calculate the water elevation and velocities throughout each subdomain, such as Thetis [64], ADCIRC [38], DIVAST [19], TELEMAC [35] or Delft3D [65], as well as *ad hoc* solvers such as the *qmesh* package [66] and the flow-modelling tool used for the Sihwa tidal power plant [67].

4.2.4. 3D models

In Sections 4.2.2 and 4.2.3, the 1D and 2D models assume that the horizontal scale is much greater than the vertical scale and, therefore, depth-averaged velocities are used. In contrast, 3D models include the vertical component of the water velocity by using the complete form of the Navier–Stokes (N-S) equations [65]. The N-S equations accurately describe the flow conditions in the immediate vicinity of the turbines and sluice gates, where the depth-averaged velocity assumption can be limiting. 3D models have been applied in literature by using Delft3D [65] or the Environmental Fluid Dynamics Code (EFDC) [68], which also allows for the study of water salinity, sediment transport and biogeochemical processes. 3D models are rarely found in operational optimisation literature for tidal barrages, due to the high computational burden associated with the computation of approximate numerical solutions of the N-S equation.

4.3. Basin

The available potential energy of a tidal barrage scheme is determined by the enclosed volume of water in the basin. Therefore, it is necessary to correctly model the bathymetry of the basin to account for the changes in area and volume, at different basin levels. Marine topographic data to determine the depth of the water bed in a certain location can be obtained from the Edina Digimap Service [43], LiDAR [64], GEBCO [35] or EMODnet [14].

The bathymetry data is then combined with a hydrodynamic model to calculate the inner and outer water levels, and available head, at each instant in time. The resolution of the bathymetric data depends on the available information from the site and is usually higher than that used for the unstructured meshes of the hydrodynamic model. In the case of the 0D model, the bathymetry data of the basin is used (or approximated) to create a depth/area curve. This corresponds with the term $A_b \equiv A_b(n_i)$ in Eq. (6) (see also [48]). A simplified approach is to consider that the basin has vertical walls and the wetted surface area inside the basin is hence constant [69]. The vertical walls assumption can give a reasonable approximation of the generated energy in sites with no substantial wetting and drying processes. However, the vertical walls assumption gives a symmetric result for ebb and flow generation when, in reality, the basin usually impounds more water volume at the top of the basin, favouring ebb generation over flood generation, as discussed previously in Section 3.2.

4.4. Turbine types and models

The most commonly used turbine in tidal barrage schemes is the bulb turbine, which is a specific configuration of a Kaplan turbine, where the generator is contained in a large bulb centred in the water pipe. Bulb turbines have high efficiency for low heads, reaching peaks of around 90% [15]. The only other turbine type used in a tidal barrage plant is the Straflo turbine, in the Annapolis Royal Generating Station (Section 3.4.6). Straflo turbines have fixed runner blades, which decrease capital and maintenance costs compared to bulb turbines, but also lower the peak efficiency and restrict the water flow to only one direction, limiting the operation to one-way generation [15]. On the other hand, bulb turbines can be operated bidirectionally, and in double or triple-regulation mode. Double-regulated bulb turbines have adjustable guide vanes and runner blades that can be manipulated to control the water flow through the turbine and maximise efficiency as the head changes. Triple-regulated turbines also include torque control to vary the turbine speed and increase the flexibility of turbine operation.

Most published studies focus on double-regulated bulb turbines, although, recently, triple regulation has been proposed for the turbines at the Swansea Bay Lagoon [70]. The guide vanes in the turbines are commonly unidirectional, which means that the flow can only be controlled in one direction. As a result, the reverse flow efficiency can drop to around 70%, compared with the 90% efficiency that the turbines can achieve in direct flow [71], with the result that, during two-way generation, the efficiency will be significantly lower in one direction.

The power output from the turbine is typically defined by 'Hill' charts, provided by the turbine manufacturer, which represent the static operating points of the turbine. The Hill chart consists of a plot of the unit speed n_{11} as a function of the unit discharge Q_{11}, for different values of efficiency, wicket gate opening, and blade pitch, as seen in Fig. 10. Q_{11} (in m^3/s) and n_{11} (in rpm) are parameters derived from turbine affinity laws [72]; hence, these depend on the turbine diameter, and can be used for different sizes of turbines. Fig. 10 shows that, for a given value of n_{11}, there are values of Q_{11} and turbine efficiency η_t that maximise the corresponding power output. It should be noted that Hill charts *do not account* for cavitation effects, as it is assumed that the turbine is sufficiently submerged.

The unit speed n_{11} and unit discharge Q_{11} are calculated as:

$$n_{11} = \frac{nD}{\sqrt{H}}, \quad Q_{11} = \frac{Q_t}{D^2\sqrt{H}}, \tag{9}$$

with

$$n = \frac{2f}{N_p}60, \tag{10}$$

and where D is the turbine diameter (in meters), H is the head (in meters), n is the turbine speed (in rpm), f is the grid frequency (in Hz), and N_p is the number of generator poles. Note that, when operated in double regulation, *i.e.* by adjusting only the guide vanes and runner blades of the turbine, the speed n is a fixed value. In triple regulation, n and n_{11} vary as the torque on the turbine is manipulated.

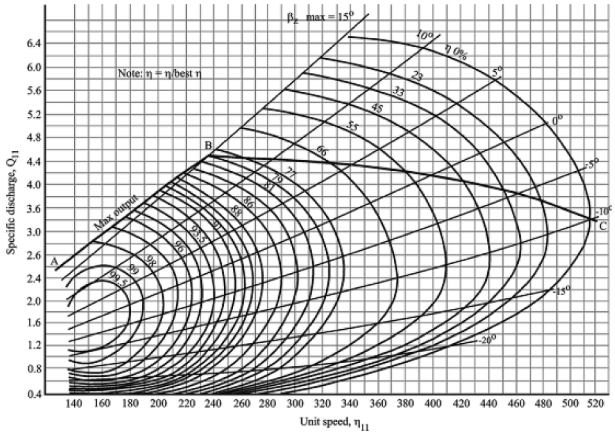

Fig. 10. Example of a Hill chart for a bulb turbine [73].

Note that it is not common to have open access to Hill charts, as they provide commercially sensitive information. Thus, the models used in literature are often generic or have limited details regarding the performance of the turbine. A particularly relevant case can be found in [6], which includes a Hill chart from a double-regulated bulb turbine created by Andritz Hydro exclusively for their research.

In particular, the mechanical power output of a turbine is calculated as:

$$P_t = \rho g \eta_t Q_t H, \tag{11}$$

where ρ is the water density (in kg/m^3). The unit speed n_{11} is calculated using Eq. (9), and is used as an input in the Hill chart to define the unit discharge Q_{11} at the maximum power point, and the corresponding turbine efficiency. The Hill chart can be digitised to approximate the maximum output curve for the unit discharge and the efficiency with the following equations [6]:

$$\begin{aligned} Q_{11} &= \begin{cases} 0.0166 n_{11} + 0.4861 & \text{if } n_{11} < 255 \\ 4.75 & \text{if } n_{11} > 255, \end{cases} \\ \eta_t &= -0.0019 n_{11} + 1.2461. \end{aligned} \tag{12}$$

The turbine flow Q_t is then calculated using Eq. (9). The mechanical power P_t can be calculated with the head, flow and efficiency, as in Eq. (11). As a result, the maximum power and discharge curves for a specific turbine can be created as in Fig. 11, which can be used to determine the operation point for a given head instead of the Hill chart [24]. It can be seen that power increases almost linearly with the head until the corresponding rated head h_{rated} is achieved. For values of head larger than h_{rated}, the maximum power capacity of the turbine is reached, and the water flow that maximises the efficiency decreases.

In tidal barrage schemes, reversible bulb turbines can be operated as pumps with the purpose of increasing the head, resulting in a higher energy output during the operating cycle [26]. The curves from Figs. 10 and 11 can also be used to model the operation of the turbine as a pump. The maximum operating head during pumping is usually much lower than the turbine rated head, which means that the pumping operation is indeed within the low-efficiency range.

The turbine orifices can also operate in sluice mode when the turbine is idling. In this case, the flow through the turbine is calculated by the orifice flow equation [38]:

$$\begin{aligned} Q_t &= G_\epsilon \sqrt{2gH}, \\ G_\epsilon &= \sum_{i=1}^{N_t} C_{Di} G_i, \end{aligned} \tag{13}$$

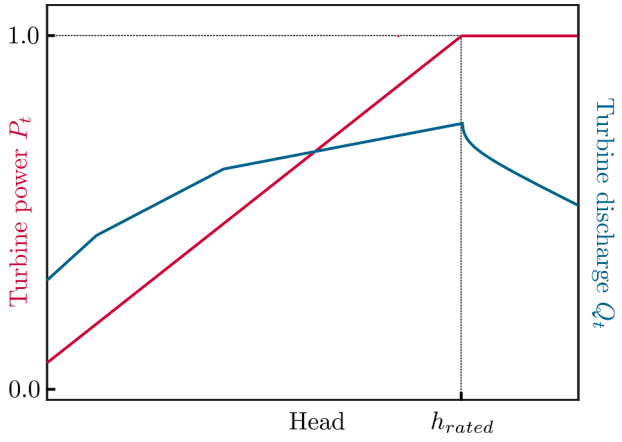

Fig. 11. Example of power and discharge curves as functions of head, for a bulb turbine. P_t and Q_t are in per unit with respect to the turbine rated power and discharge.

where N_t is the number of turbines, C_{Di} is the discharge coefficient of the i-th turbine duct, and G_i is the corresponding area. Eq. (13) can also be used to estimate the turbine flow when the turbine is generating as in [74], where the efficiency is approximated by an empirical equation of the form:

$$\eta_t = \left[1 - \left(\alpha \left| 1 - \beta \frac{Q}{Q_n} \right|^{\chi}\right)\right] \delta, \tag{14}$$

with α, β, χ and δ dimensionless scaling factors, and Q_n the rated discharge of the turbine (in m^3/s). [9] compares the use of the Hill chart to calculate the turbine efficiency to the use of Eqs. (13) and (14), and shows that both methods deliver similar results.

[46] uses a linearised form of Eq. (13), for heads lower than 7 m, to model the discharge through the turbines while idling, *i.e.*

$$Q_t = K_t G_\epsilon H, \tag{15}$$

where K_s is a design coefficient. Moreover, to model the turbines during generation mode, [46] uses a piecewise linear function to approximate the turbine power and flow characteristic shown in Fig. 11.

As seen in Fig. 10, the Hill chart allows to control wicket gate opening, blade pitch, and turbine speed in the turbine model, in order to define the operating point of the turbine. The only study that explicitly manipulates these variables is [10], where a triple-regulated turbine is used. The study shows that this flexible turbine operation increases energy generation by at least 5%, compared to operating the turbines at full load (*i.e.* at maximum discharge for each head, as illustrated in Fig. 11). This means that, although easy to implement, restricting the turbine operation to one degree of freedom (such as in Eqs. (12) and (14)) can considerably constrain the operation of the turbine, compared to modelling the full range of turbine actuators.

4.5. Sluice gates

Sluice gates allow the water to flow through the embankment in order to create the required hydraulic head. They are designed to maximise the water discharge capability, and therefore minimise the number of sluices needed, which in turn reduces construction costs. For this purpose, the optimal geometry of the sluice gates should be carefully studied, see *e.g.* [75]. In particular, the discharge through the sluice gates is given by the orifice equation

$$Q_s = A_s C_d \sqrt{2gH}, \tag{16}$$

where A_s is the sluice area (in m^2) and C_d is the discharge coefficient. To avoid the non-linear characteristic of the flow through the sluice gates (and idling turbines), given by Eq. (16), [46] proposes a linearised equation with the following structure:

$$Q_s = K_s A_s H, \tag{17}$$

where K_s is chosen to approximate the sluice gates flow for heads lower than 7 m.

4.6. Generator, transformer and drive train

The ultimate goal of the tidal barrage scheme is to convert potential energy into electrical energy. As mentioned in Section 4.4, bulb turbines contain a synchronous generator within the bulb which, in some cases, is coupled to the shaft by a gearbox. The generators are connected to the power grid by means of transformers, which can vary in number according to the chosen layout of the electrical installation. In the case of triple-regulated turbines with variable speed, an induction generator with a variable speed drive is used instead of a synchronous generator, which is coupled to the grid with an electronic power converter.

The electrical machines and drive train are typically modelled by

adding a constant efficiency coefficient to the power equation, *i.e.*

$$P_e = \eta_{gen}\eta_{tr}\eta_m P_t, \tag{18}$$

where η_{gen} is the generator efficiency, η_{tr} is the transformer efficiency, and η_m represents the mechanical losses from the drive train and gearbox.

5. Optimisation and control of tidal barrage operation

This section addresses the core of this study, *i.e.* the use of optimisation and control techniques for optimal operation of tidal barrages. In particular, the control objective for a tidal barrage plant is to maximise (or minimise) a certain performance function by optimal operation of the turbines and sluice gates composing the barrage. The turbines are operated by manipulating blade pitch, wicket gates, and turbine torque (depending on whether the turbine is double-regulated or triple-regulated) to control the flow through the turbine. The flow through the sluices is actuated by a servomotor that essentially opens and closes the sluice gates according to a defined schedule. A general formulation of an optimal control problem (OCP) for the operation of a tidal barrage power plant can be given as follows:

$$\begin{aligned} v^{opt} = \quad & \underset{v\in\mathscr{V}}{\operatorname{argmax}} \int_{t_1}^{t_2} f_o\left(v,t\right)\mathrm{d}t \\ & \text{Subject to :} \\ & \text{Tidal barrage dynamics, as per Section 4, and} \\ & \text{Physical constraints,} \end{aligned} \tag{19}$$

where v is the vector of manipulated variables (control inputs), assumed to belong to a certain admissible function space $\mathscr{V}$, f_o is the control objective, and $[t_1,t_2], t_1 < t_2$, is the time window under analysis, typically composed of a certain number of tidal cycles. As is standard in the vast majority of OCPs, the solution to OCP (19), with a generic objective f_0, is of a feedforward nature [76], where the manipulated variables are 'precalculated', by leveraging a mathematical model of the tidal barrage process and then implemented *a posteriori* to control the operation of the barrage.

The dynamic constraint in the OCP (19), *i.e.* the model representing the tidal barrage itself, includes the dynamic behaviour of the different components of the system. In particular, the barrage dynamic model incorporates a description of the process hydrodynamics, turbines, sluice gates, and any associated electrical machines. Using the notation defined in Section 4 for each different subsystem composing the barrage, the dynamic constraint in the OCP (19) is normally given in terms of a map $\mathscr{H}$ relating each component of the barrage to the instantaneous hydraulic head, *i.e.*

$$H \leftarrow\!\shortmid \mathscr{H}(\mathcal{H},\mathcal{B},\mathcal{T},\mathcal{S},\mathcal{E},n_o), \tag{20}$$

where the explicit definition of $\mathscr{H}$ depends upon the considered modelled components and assumptions adopted (see the discussion provided in Section 4).

With regards to the OCP in (19), as discussed within the remainder of this section, the control objective function f_0 is normally written in terms of energy absorption from tidal variation, with additional terms that might include (electrical) energy demand and/or economical considerations, *i.e.* the solution of the OCP is mostly influenced by the tide dynamics (see Section 4). As such, the relatively slow change in tidal elevation, which is effectively dominant in the tidal barrage system, implies that the faster dynamics of the turbines $\mathscr{T}$, sluice gates $\mathscr{S}$ and electrical machines $\mathscr{E}$ can be generally disregarded (or simplified) when solving the OCP (19) (see also the discussion in Section 4), with a minimal impact on the optimality of the solution. In other words, the dominant dynamics in the OCP are those related to the hydrodynamic processes $\mathscr{H}$ occurring inside and outside the basin. Moreover, the slow variation of the tidal elevation considerably reduces the computational severity for real-time optimal control of the barrage, enabling the use of a broader range of control strategies. It should be noted, however, that the tidal elevation can be affected by stochastic perturbations such as variations in weather conditions (air pressure, wind direction and strength), as discussed in Section 2.1, although these perturbations are relatively small compared to the tidal elevation due to gravitational effects, *i.e.* the process can be considered to be deterministic for most practical purposes.

Fig. 12 shows a block diagram representing the operation and control of a tidal barrage scheme. The external input is the tidal height, usually modelled as a sinusoid or sum of sinusoids, *i.e.* the tidal constituents, as discussed in Section 4.1. The tidal level and inner basin level determine the instantaneously available head in the vicinity of the barrage. As per the definition of the OCP in (19), the hydrodynamic model of the barrage is used within controller synthesis to determine the operating mode of both the turbines and sluice gates. In particular, the available head, and operating mode of the turbines and sluice gates, produce a required turbine flow Q_t and sluice gates flow Q_s, which combined give the total flow through the barrage and result in a variation of the water elevation inside the basin.

Table 4 provides an overview of the different approaches available in the literature for solving the OCP of tidal barrages and lagoons, according to the definition provided within this section. These references, and associated techniques, are discussed in detail in the following paragraphs. (see Table 5).

5.1. Optimal control problem formulation

This section describes in detail the different OCP formulations considered within the state-of-the-art of optimal tidal barrage operation, providing an account of the elements involved in the OCP (19), for each study presented in Table 4. In particular, control objectives, in terms of the performance function f_0, are discussed in Section 5.1.1, while manipulated variables (and associated physical constraints) are addressed in Section 5.1.2. Finally, Section 5.1.3 discusses the main modelling assumptions used for the formulation of the OCP and, hence, the final computation of the optimal operation sequence of the tidal barrage system.

5.1.1. Control objectives

The periodic and highly predictable nature of the tidal elevations, combined with the inherent storage capability of the basin, allows tidal barrages to be operated for different objective functions, which can be considered to be solved in a virtually deterministic fashion. Table 3 lists several possible control objectives that can be considered within the tidal barrages OCP, according to the state-of-the-art. As can be appreciated from Table 3, in general, the control objective is directly linked to maximisation of energy absorption, to achieve a high income for the power plant, and a low levelised cost of electricity (LCoE). In particular, this objective can be written, with f_0 in (19), as

$$f_0(v,t) \equiv P(v,t), \tag{21}$$

where $P(v,t)$ denotes the power generated by the turbines.

An alternative approach, pursued within the literature, is to consider the hourly electricity market prices to maximise the revenue of the power plant by generating when the prices are higher [46], *i.e.*

$$f_0(v,t) \equiv p(t)P(v,t), \tag{22}$$

where $p(t)$ is the hourly market electricity price. Note that the high predictability of the tidal range resource, and the flexibility of tidal barrages, enable tidal barrage power plants to participate in energy trading schemes such as the Day Ahead Market (DAM), with lower risk than other renewable power plants [77]. In particular, [77] considers

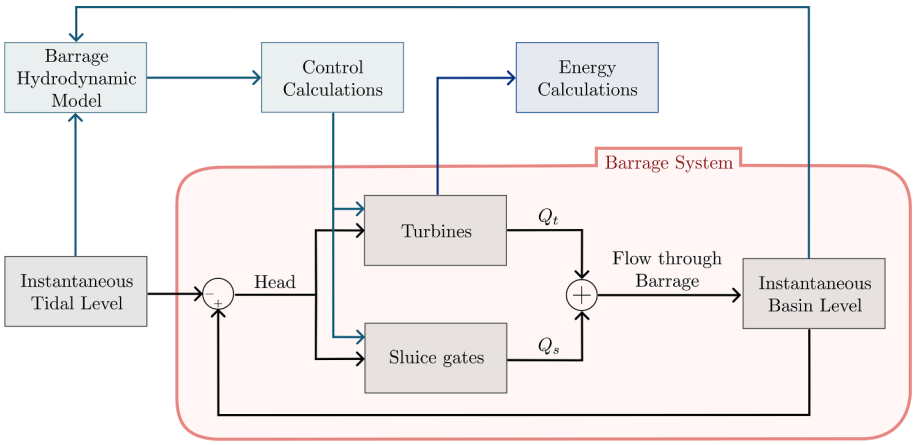

Fig. 12. Block diagram describing the model for the control of a tidal barrage.

Table 3
Possible control objective functions for tidal barrages OCP.

	Control objective	Objective function f_0
RM	Revenue maximisation	$p(t)P(\boldsymbol{\nu},t)$
PM	Profit maximisation	$p(t)P(\boldsymbol{\nu},t) - C(\boldsymbol{\nu},t)$
DM	Demand matching	$-[P(\boldsymbol{\nu},t) - D(t)]$
EM	Energy maximisation	$P(\boldsymbol{\nu},t)$
CG	Continuous generation	$Wp(t)P(\boldsymbol{\nu},t) - C(\boldsymbol{\nu},t)$
LM	LCoE minimisation	$\frac{P(\boldsymbol{\nu},t)}{C(\boldsymbol{\nu},t)}$

not only the historic hourly energy price, but also the potential impact of the analysed tidal lagoon schemes on the hourly market price, by calculating an adjusted price $p_{adj}(t)$ proportional to the energy generated by the tidal lagoons under study.

The operation and maintenance cost (OpEx) of the turbines can also be included within Eq. (22), as done in [78]:

$$f_0(\boldsymbol{\nu},t) \equiv p(t)P(\boldsymbol{\nu},t) - C(\boldsymbol{\nu},t), \tag{23}$$

where $C(\boldsymbol{\nu},t)$ denotes the associated OpEx. Note that, in [78], the manipulated variable is the number of operating turbines N_t; therefore, the OpEx depends only on N_t, which can be seen as rather simplistic. A more realistic scenario, yet with an increased order of complexity,

Table 4
Operational control strategies found in literature. (*) Generic nonlinear solver. (**) Not declared explicitely.

Reference	Optimisation type	Control objective	Barrage design optimisation	Manipulated variables								Constraints							Assumptions						Optimal control formulation	Optimal control solver
				τ_i	N_t	N_s	Q_t	Q_s	h_s	h_f	$\mathbf{m}_t$	τ_i	N_t	N_s	Q_t	Q_s	n_i	h_s	h_f	Same operation in every phase	All turbines and sluices operate equally	Fixed operating mode	Instantaneous transition between operating phases	No overlap between phases	Sequential operation		
[43]	OC	EM, RM		×								×								×	×				×	Two-cycle optimisation	GB, BH
[6]	FP	EM	N_t, C_t, d_t						×											×	×	×	×	×	×		(*)
[7]	OC	EM	N_t	×								×								×	×				×		GB
[39]	FP	EM, DM							×											×	×	×	×	×	×		(*)
[78]	OC	PM	N_t, λ	×	×							×	×							×		×		×	×		GB
[64]	OC	EM, CG		×								×								×	×	×	×		×	Two-cycle optimisation	GB
[77]	OC	EM, RM	N_t, N_s	×	×							×	×							×	×	×	×		×	Two-cycle optimisation	GB
[79]	FP	EM	N_t						×											×	×	×		×	×		(**)
[8]	OC	EM							×	×								×	×	×	×	×	×	×	×	Two-cycle optimisation	GA
[42]	OC	EM	N_t, N_s						×	×								×	×	×	×	×	×	×	×	Two-cycle optimisation	GA
[80]	OC	EM							×	×								×	×	×	×	×	×	×	×	Two-cycle optimisation	(**)
[49]	FP	EM	N_t, d_t						×											×	×	×	×	×	×		(*)
[11]	OC	EM			×	×						×	×							×			×			Model predictive control	(*)
[12]	OC	EM					×	×							×	×	×				×					Moment-based control	(*)
[34]	OC	EM	N_t		×										×		×	×	×	×		×	×	×	×		GA
[48]	OC	EM		×											×	×					×	×				DRL	PPO
[13]	OC	EM							×	×								×	×		×	×			×	RL	PPO
[69]	FP	EM		×																×	×	×	×	×	×		MILP
[24]	FP	EM							×	×										×	×	×	×	×	×		(**)
[81]	OC	EM					×								×						×			×			(**)
[9]	OC	RM	N_t, N_s, d_t, d_h, w_s		×	×						×	×				×			×		×	×	×	×		PSO
[46]	OC	EM, RM			×							×								×		×	×	×	×		MILP
[10]	OC	RM			×				×	×	×	×		×			×	×	×				×		×	PCA	EA

Table 5
List of abbreviations from Table 4. Abbreviations for the control objectives can be found in Table 3

OC	Optimal control	EA	Evolutionary algorithm	Q_t	Turbine flow
FP	Fixed parameter	MILP	Mixed-Integer Linear Programming	Q_s	Sluice gate flow
GB	Gradient-based algorithm	τ_i	Duration of operational phases	n_i	Basin water level
BH	Basin–hopping algorithm	N_t	Number of turbines	h_s	Starting head
GA	Genetic algorithm	N_s	Number of sluice gates	h_f	Finishing head
PSO	Particle swarm optimisation	d_t	Turbine diameter	λ	L/A, where L is the length of the
(D) RL	(Deep) reinforcement learning	d_h	Turbine hub diameter		impoundment and A is the basin area
PPO	Proximal policy optimisation	w_s	Sluice gate width	$\mathbf{m}_t$	Vector of turbine actuators
PCA	Principal component analysis				(blade pitch, wicket gate opening and speed)

would be to include the operation and maintenance cost of other main components of the barrage, such as *e.g.* sluice gates or ship locks, to give a more precise total OpEx figure to be considered in the OCP. In fact, a more general performance objective can be stated as:

$$f_0(v,t) \equiv \frac{p(t)P(v,t)}{C(v,t)}, \tag{24}$$

which essentially corresponds to minimisation of LCoE, assuming a given (fixed) capital cost (CapEx).

As described in [43], income maximisation can also be linked with demand matching, given the correlation between energy price and energy demand. A general formulation of a demand-matching control objective is of the form

$$-f_0(v,t) \equiv P(v,t) - D(t), \tag{25}$$

where $D(t)$ is the instantaneous electricity consumption corresponding to a certain demand (*i.e.* restricted to a certain location or type of consumer). Note that a negative sign is introduced in Eq. (25) simply to denote minimisation (as opposed to the maximisation formulation posed in the OCP (19)). Demand-matching objectives are not explicitly used in the literature; the closest example of a demand-matching strategy is presented in [39], where, instead of using the formulation in Eq. (25), the tidal barrage plant is operated so that the turbines generate electricity only during periods in which the instantaneous electricity demand is higher than an average electricity demand trend-line. [39,43] show that both income maximisation and demand matching often result in lower energy output of the power plant.

Moreover, given the inherent storage capability of tidal barrages, the operational strategy can be to provide constant power output to the grid. This can be achieved with linked-basin barrages, as per the discussion provided in Section 3.1, although little has been written about the operation of linked barrages. A generalised formulation of the continuous generation objective function, presented in Eq. (23), can be written in the form

$$f_0(v,t) \equiv Wp(t)P(v,t) - C(v,t), \tag{26}$$

where W is a weighting coefficient that essentially scales down the instantaneous power, with the purpose of flattening the power output throughout the time interval considered within the OCP formulation, hence achieving a more continuous power curve. The weight W can be either constant (fixed), or a function of time and/or the set of manipulated variables v. For instance, in [78], where the operation of a linked-basin barrage is optimised, W is formulated as follows:

$$W = \frac{1}{1+\beta_p\sigma_p}, \tag{27}$$

where σ_p is the standard deviation of the power generated at any point in time over a tidal cycle, and β_p quantifies the importance of constant power output. By using the standard deviation of the power, the aim is to achieve a homogeneous power output throughout all tidal cycles over a year. For low values of β_p, the optimal number of operating turbines is always equal to the maximum available, whereas, for increased values of β_p, the turbines are turned on and off to maintain a certain head between the low water basin and high water basin, thus extending the generation periods. A drawback of this formulation is that minimising σ_p over the whole year is equivalent to having the same instantaneous power all year, which might result in below-optimal power output during spring tides.

An alternative way of achieving constant power, considered within the literature, is to jointly operate several tidal barrages located in different sites where the tides have phases that can complement each other. [64] studies the optimal operation of three tidal range schemes in the Severn Estuary, where the phase difference between the tides allows for a consistent power supply throughout the day. The optimisation is performed in two stages: First, a maximisation of the time t_g in which at least one plant is generating is pursued. In particular, the function t_g weights the cost of operating at least one of the tidal range schemes, in accordance with the availability of the resource at each plant. Once it is assured that t_g can be effectively equal to the period of the tidal cycle, the minimum cumulative power output for constant generation $\wedge P$ from all the plants is maximised. This two-stage optimisation can be written as:

$$\begin{aligned} &\text{First stage}: \quad \max_{v} t_g\left(v\right), \\ &\text{Second stage}: \quad \max_{v} \int_0^{t_g} \wedge P\left(v,t\right) \mathrm{d}t. \end{aligned} \tag{28}$$

This coordinated operation requires a more complex and computationally demanding optimisation formulation, but results in a more efficient use of the installed capacity, compared to that of a standard linked-basin scheme.

5.1.2. Manipulated variables

The standard operation of a tidal barrage plant is given by actuation of turbines and sluice gates along the embankment. Therefore, using the turbines and sluice gates flows, Q_t and Q_s, as manipulated variables for control purposes, can be seen as the most straightforward option, as opted for, for example, in [81]. However, other parameters/design specifications can be considered in the definition of the OCP (19). For instance, several studies, such as [78], use the effective number of turbines and sluice gates, N_t and N_s, which is an indirect way of controlling both turbines and sluice gates flows.

Another way of defining the operation of a barrage scheme is in terms of the starting head h_s and finishing head h_f (see Fig. 5). In particular, h_s is the head at which the turbines start generating, while h_f is that at which the turbines effectively stop the generation process. h_s and h_f are used as manipulated variables in several studies, such as [13]. In some cases, h_f is assumed to be equal to the turbine minimum head, to reduce the number of variables to be optimised [6]. In [80], a starting pumping head h_p is also added to determine the head at which the turbine starts operating as a pump. The use of h_s and h_f actuates directly on the turbines, and indirectly on the sluice gates, by assuming that, before generation starts and after generation finishes, the sluice gates are either open or closed (holding). In [10], apart from using h_s, h_f and N_t, the pitch, gate opening and speed of the turbines are manipulated to get a desired turbine discharge.

Some studies, such as [43], also use a time vector τ that determines the times when the turbine starts and stops generating (or pumping), and the times when the sluice gates open and close. This, in turn, implies that the power $P(v,t)$, as defined per the control objectives described in Section 5.1.1), is piece-wise continuous in t. [48] does not explicitly use τ but rather a discrete variable that determines the action of the turbines and sluices at each time, which could be considered equivalent.

5.1.3. Standing assumptions when solving the optimal control problem

For the purpose of simplifying the formulation of the tidal barrage OCP itself and its associated solution, the typical operation of a tidal barrage plant is commonly divided into several distinct phases, depending on the operating mode, as can be appreciated in Fig. 5: *Generating*, *holding*, *filling*, and *emptying*. Note that the generating phase can overlap with the sluicing (filling or emptying) phases, meaning that the sluice gates can be effectively open during generation. Also, the turbines can be used for free filling and emptying, or as pumps. The duration of each phase during one tidal cycle determines not only the energy that is extracted during that cycle, but also the available head on the following one. Therefore, the control strategy of one cycle impacts the overall energy that can be extracted at the next, adding an additional

degree of complexity to the process of solving the associated control problem.

There are a number of standing (simplifying) assumptions that are commonly adopted within the literature when formulating the tidal barrage operation optimisation, namely:

A1. Turbines and sluices have the **same operation in every phase**: The flow through the turbines is either constant or is defined by the operating head (for instance, by using the maximum power curve or the maximum efficiency curve from the Hill chart), and sluice gates always operate either fully open or fully closed.
A2. **All turbines/sluices operate 'equally'**: there is no distinction in the operation of each individual turbine and sluice gate. All the turbines operate at the same water flow, and all the sluice gates move together.
A3. **Fixed operating mode**: The operating mode, *i.e.* ebb, flood or two-way with or without pumping, is predefined.
A5. **Instantaneous transition between operating phases**: Each operating phase starts and stops instantaneously, without considering any potentially significant dynamics associated with the sluices and turbines. Note that, in the cases in which transitions are not instantaneous, these are often approximated with ramp functions [25] instead of using a more comprehensive model of turbines and sluices.
A5. **No overlap between phases**: The operating phases are distinct from each other, *i.e.* generation, sluicing and pumping do not overlap in time.
A6. **Sequential operation**: There is a predefined order in which each phase takes place.

The simplifying assumptions considered in the optimisation have an impact on the set of variables that can be manipulated. For instance, using h_s and h_f, within the formulation of the OCP (19), can give acceptable results with mild computational effort, but can only be performed by assuming A3, A5 and A6. Using the duration of each phase (τ) as part of the manipulated variables gives more flexibility since, by setting the lower bound to zero, the operating mode can be dynamically adjusted. However, the number of manipulated variables increases when compared to using starting and finishing heads only; moreover, using τ, assumes A6. By changing N_t and N_s, the overall flow through the barrage is controlled without the need to establish the operating phases in advance, giving more flexibility to the operation, although A1 is adopted as a standing assumption. Individually manipulating turbine and sluice gate flows gives the most flexibility, though this is not typical of the studies reported in the literature, ostensibly due to the underlying complexity of the associated OCP.

5.2. Fixed-parameter operation

In tidal barrage operational optimisation, the predominant approach observed within the state-of-the-art literature is fixed parameter, or non-flexible, operation. In particular, the parameters that define each operational phase of the barrage are selected based on a preliminary analysis, such as an iterative offline optimisation, or based on previous experience. Once the parameters are defined, the operation of the barrage is simulated using the selected set of values. The operating mode, *i.e.* ebb, flow or two-way generation, with or without pumping, is also predefined.

An early and noteworthy study on tidal barrage optimisation can be found in [82], where an analytical model is used to describe a tidal barrage plant under a number of simplifying standing assumptions. The model is described in terms of dimensionless parameters, allowing the results to be generalised for different barrage scales. The optimisation is performed using graphic models, particularly by plotting the energy produced as a function of the finishing level (*i.e.* the basin level at the time when the generation stops) for different minimum heads. The main aim of [82] is to give an approximate idea of the behaviour of a tidal barrage under different operating conditions, rather than optimising its operation in detail. The study shows that two-way generation theoretically yields more energy than one-way, assuming the same installed capacity, and analyses how the operating head, and optimal starting and finishing heads, vary with different operating modes. [69] proposes another analytical control formulation for the dispatch of a tidal barrage and compares it with the one in [82]: both give similar results in terms of energy output, but the model in [69] has a much faster computational time.

In [79,49], the starting head is chosen to maximise the overall annual energy output, meaning that is constant for every tidal cycle, regardless of the variation in tidal amplitude. This operation has the disadvantage of not taking into account that, during neap tides, there is less time to fill or empty the basin, so the optimal starting head varies from that of spring tides. On the other hand, in [39], the optimal starting head is calculated for different tidal ranges, which allows more flexible operation of the barrage and a higher energy output.

5.3. Optimal control strategies

In contrast with fixed parameter optimisation, optimal control algorithms can account for the temporal tidal variations more accurately, by optimising the manipulated variables accordingly. This allows not only a higher flexibility in the definition of the operating parameters, but also for dynamic selection of the operational strategy (ebb, flood or two-way generation, with or without pumping).

An illustrative example of the energy increase between fixed-parameter and optimal operation can be found in [7]. First, the manipulated variables are optimised assuming uniform operation of the barrage throughout the year, and these values are then used as initial conditions for flexible operation optimisation, resulting in energy gains of over 28%. A similar analyses can be found in [80].

Following the formulation presented in Section 5.1.1, recall that the energy maximising OCP for the operation of a tidal barrage can be essentially posed as:

$$\max_{v} \int_{iT}^{(i+1)T} P(v,t)\,\mathrm{d}t, \tag{29}$$

where T is the period of a tidal cycle (for the semi-diurnal cycle, the period is 12.42 h, as seen in Section 2.1), and i defines the tidal cycle under consideration. The operation of the tidal barrage during one tidal cycle determines the available head for the following cycle; hence, solving the optimisation problem for each cycle separately might not give the optimal result for the complete time window under analysis. Several strategies can be found within the literature, which consider the impact of the operation of one cycle on the overall operation within a given time window. In particular, assuming that the process is effectively deterministic and periodic, one way is to consider two tidal cycles as part of the optimisation problem: A cycle where the operating variables are manipulated, and the following cycle, where the operation is predefined, *i.e.*

$$\max_{v} \int_{iT}^{(i+1)T} P(v,t)\mathrm{d}t + \int_{(i+1)T}^{(i+2)T} P(t)\mathrm{d}t. \tag{30}$$

This approach is taken in [64,43], where the optimal control problem includes each subsequent cycle. First, the duration of the generation phase (τ) is assumed to be fixed for all tidal cycles, and optimised to maximise the energy over the selected time window. Then, the control problem is formulated with τ_i (the duration of the generation phase for each semi-diurnal tidal cycle i) as the control variable, but the objective is set to maximise the energy generated over two consecutive cycles, assuming that, in the second cycle, the duration of the generation phase is that resulting from the previous fixed parameter optimisation, given

by τ. [43] shows that considering the following cycle in the optimisation problem increases the energy output between 1% and 3%.

[80] presents two optimisation strategies: one in which the operation is optimised for every semi-diurnal tidal cycle (denoted by ET) or for half of a semi-diurnal tidal cycle (denoted by EH), individually, and another where the next tidal cycle or half tidal cycle (denoted by ETN and EHN, respectively) is considered. The results show that, by taking into account the next tidal cycle in the optimisation (ETN and EHN optimisation), the generated energy increases with respect to the single-cycle optimisation (ET and EH), although with a marginal gain in performance (about 1%).

On the other hand, [11] uses nonlinear model predictive control (NMPC) to control the percentage of turbines connected to the grid. The NMPC method predicts how the system will evolve over a certain time horizon to iteratively optimise the control for a given performance criterion, in a standard receding-horizon fashion. Applied to barrage operation, NMPC considers a certain number of consecutive semi-diurnal tidal cycles, depending on the selected prediction horizon, instead of just a single cycle.

In [12], a moment-based framework is used for the parameterisation of the energy-maximising optimal control problem for a tidal barrage scheme. The optimisation is carried out over the whole time window under consideration, which means it includes all semi-diurnal tidal cycles of the time window, though [12] considers only one semi-diurnal tidal constituent.

By considering two consecutive semi-diurnal cycles, it is clear that better optimisation results can be achieved than by solving for each tidal cycle separately. Note that, in the studies that apply this method, the operation of the following cycle is not optimised, but uses a predefined control input vector. On the other hand, NMPC optimises the manipulated variables for the complete prediction horizon, which can produce a more effective solution for the control problem (*i.e* closer to the actual optimal value of the associated OCP). Moreover, both NMPC and moment-based control allow the use of several consecutive tidal semi-diurnal cycles, instead of just two consecutive cycles. The NMPC and moment-based frameworks have a number of advantages, including efficient computational capabilities and the ability to effectively handle physical system constraints, and allow for flexible operation of turbines and sluices. Moment-based control adopts the assumption that the barrage operation is periodic with the same fundamental frequency as the tide, which allows for efficient computation of the optimal steady-state manifold associated with the controlled barrage system, though this periodicity assumption might be a limitation on the flexibility of the solution.

The solver used for the transcribed optimisation problem should be able to handle nonlinear programs with constraints and discontinuities (for instance, the orifice equation of the sluice gates is a square-root function). Nonlinear gradient-based algorithms are applied in a number of paper, such as [7], but have the disadvantage that the selection of the initial conditions can lead to convergence to a local optimum instead of a global optimum. In this sense, [43] compares two cases: Using a result from fixed-parameter optimisation as an initial condition, and a global basin–hopping algorithm [83] is then applied, where random values are used for initialisation. The results show that the basin–hopping algorithm yields between 4% and 6% more energy than a traditional gradient-based approach. In [8,42], genetic algorithms (GA) are used to solve the transcribed optimal control problem. During each iteration (generation), a number of operating schemes (chromosomes) are created and go through mutation, recombination and selection processes, where the manipulated variables (genes) are modified. The schemes where the generated energy is higher (the 'fittest', assuming that the objective, or fitness, function is energy maximisation) become the following generation. The results from the optimisation with GA in [42] are compared with the EHN optimisation using a grid search algorithm, and, with the same resolution, the study found that using the GA performs the optimisation faster.

On the other hand, [9] uses a particle swarm optimisation (PSO) algorithm, which is also a population-based stochastic optimisation technique where the velocity and position of each particle from a population is updated in each generation to achieve the best solution. The results from the PSO in [9] are compared with those using a GA, with the former algorithm giving a higher energy output. That is to say that, in this case, PSO is better able than GA to find the global optimum, considering that the transcribed OCP is formulated as a non-convex program. [9] also shows the relevance of choosing an appropriate optimisation algorithm for the tidal barrage OCP.

Another population-based algorithm applied to tidal barrage optimisation is the Evolutionary Algorithm (EA) [10]. As mentioned in Section 5.1.2, the study uses a large number of manipulated variables, making the associated OCP quite complex. The EA is combined with a principal component analysis technique (PCA) for the purpose of model reduction. Though [10] does not present any detail regarding the implementation and performance of the algorithm, it can be pointed out that the EA tool is able to provide a global optimum, considering a highly complex barrage model.

Reinforcement Learning (RL) and Deep Reinforcement Learning (DRL) are applied in [13,48], respectively. In RL, the turbines and sluice gates are operated by an 'agent', who is trained with a tidal elevation input from the site. After training, which only needs to be done once [13], the agent can perform online control of the operation of the tidal barrage, with a resulting energy output comparable to the results from [80], although with no comparative energy gains. A distinct feature of RL and DRL is that the tidal elevation does not need to be forecasted and predefined which, if available, could account for the variations in water elevation due to stochastic weather conditions. Furthermore, [48] shows that the DRL algorithm can replicate the real operation of the La Rance power plant, which means that the solution is realistic. In [48], optimisation yields a 2,6% energy gain because the objective function is to maximise energy, whereas the La Range power plant operates with a revenue maximisation strategy.

5.4. Control co-design

Control co-design of a tidal barrage is a relevant optimisation problem in itself, particularly when the tidal plant under study is essentially still at a development stage. Optimal design of tidal barrages often consists of calculating the energy generated with a predefined operational strategy and varying a single design parameter, chosen to maximise the energy output, as for instance in [42]. In contrast, a control co-design approach includes the design parameters as part of the OCP, by explicitly accounting for the physical description of the barrage in the control formulation. In [77], a control co-design approach is used for an initial fixed-parameter optimisation, where the number of turbines is included in the vector of manipulated variables, along with the holding and generating periods. [78], in an initial stage, formulates a control co-design problem where the manipulated variables are both the time vector τ (Section 5.1.2) as well as the number of turbines N_t installed in the power plants. Nonetheless, the number of turbines is only used to solve the optimisation, for computational simplicity. To the best of the authors' knowledge, these are the only studies that formulates a control co-design problem, which leaves a path for future work in this area.

In particular, OCPs with objective functions that include CapEx and OpEx are suitable for including design parameters in the control input vector (see Eq. (19)), such as the number and capacity of turbines, sluice gate areas, sizes of the gate servomotors, and length of the embankment, among others. Examples of control co-design can be found in the literature applied to other ocean energies, such as tidal current energy (see [84] or [85]) or wave energy [86]. Control co-design can also be potentially implemented by using a Hill chart for the turbine model: As seen in Section 4.4, Q_{11} and n_{11} are functions of the turbine diameter D, which can be added as a manipulated variable, instead of considering D as a fixed parameter.

6. Perspectives and future directions

The tidal range resource has the advantage of being highly predictable compared to other renewable sources, although it can only be efficiently harnessed in a certain number of sites around the globe. Tidal barrages, compared to other ocean energy schemes, utilise mature technologies, such as bulb turbines and dams, allowing these to reach a high commercial readiness level, with several power plants actively operating around the globe.

The two main challenges that tidal barrages face are economic and ecological. The operational strategy implemented on a barrage scheme can influence both economic (in terms of energy maximisation or flexible generation during high energy price) and environmental aspects (in terms of preserving wetting and drying processes and flood mitigation). In this sense, research in optimal control of tidal barrage operation is fundamental to maximise the income of the barrage power plant while adding constraints that can incorporate environmental considerations. In order to effectively consider the environmental impacts of the barrage, a comprehensive hydrodynamic model that can be used for optimal control is needed, which is a problem that still needs to be tackled. Additionally, there is a huge unexplored potential of tidal barrages for providing ancillary services to the power systems.

6.1. The optimal control problem

Current practices in optimal control techniques applied to tidal barrages use rather simplified barrage models, leaving room for further development of more accurate (yet computationally amenable) models, so as to achieve solutions that can yield a better performance in realistic scenarios. Most studies divide the operation of tidal barrages into distinct phases, which enables the formulation of the barrage OCP in a straightforward manner, but may overly restrict the solution space and fail to achieve a global optimum. A more holistic approach to the OCP could achieve a higher performance, but potentially render the OCP formulation harder to synthesise, and solve.

Regarding the definition of the control objective itself, the vast majority of the literature on tidal barrage operation optimisation uses energy-maximising objective functions. Only a few studies focus on revenue/profit maximisation, demand matching or continuous generation. No studies were discovered which formulate the objective function as LCoE minimisation, or on the implementation of control co-design in the OCP, leaving opportunities for further research. Most studies within the current literature show the importance of considering consecutive tidal cycles in the OCP formulation, to account for the impact of barrage operation on subsequent cycles. In this sense, model predictive control and moment-based control present clear advantages [12]. In particular, moment-based control allows to exploit the periodic characteristics of the tidal elevation by implementing an efficient parameterisation of the steady-state behaviour of the underlying dynamical system. Because of the harmonic behaviour of the tidal elevation, there is plenty of untapped potential for further research on a large pool of control techniques, including *e.g.* spectral and pseudo-spectral control in tidal barrage optimisation. Furthermore, reinforcement learning techniques appear particularly suitable for online operation control [13]. Regarding the numerical solution of the associated transcribed OCP, it is shown in the literature that different algorithms can achieve different optimal solutions [9], further emphasising the rather complex nature of the underlying optimisation problem. All these considerations leave room for further analysis on the definition (objective) and transcription of the OCP itself, and the subsequent solution method pursued for optimal barrage operation.

With respect to actuators, the turbines are usually modelled using the a turbine Hill chart, and by following the maximum efficiency curve. [10] shows that, by manipulating the blade pitch, wicket gates and turbine speed individually, instead of restricting the turbine operation to the points of maximum efficiency, a more optimal solution for the barrage operation can be achieved. This leaves a path for future research on optimal barrage control with a more flexible turbine operation. Moreover, special consideration should be given to triple-regulated turbines: They require different technologies on the electrical coupling side (*i.e.* an asynchronous generator, variable speed drive and back-to-back converter), which limits the ancillary services that the generator could provide to the power grid [87]. The use of the Hill chart also allows the possibility of control co-design which, as previously discussed in Section 5.4, has been rarely exploited in tidal barrage optimisation.

6.2. Hydrodynamic and environmental considerations

On the modelling side, yet strongly connected with the solvability of the underlying OCP, the biggest challenge remains accurate (yet parsimonious) hydrodynamic modelling of the barrage. The hydrodynamic models currently exploited appear to be either too simple (*i.e.* 0D models) or too complex (*i.e.* 2D and 3D models). Only 0D models are used in the literature to solve the tidal barrage operation OCP, leaving higher dimensional models for result validation/controller calibration. Ultimately, it would be ideal to develop efficient control techniques, being able to include potentially complex hydrodynamic models, which are necessary to accurately analyse the economic viability of a tidal barrage project and evaluate its environmental impact. 2D and 3D models play an important role when it comes to project assessment, as they provide an accurate representation of the hydrodynamics of the tidal circulation [38]. High-dimensional models not only allow for the computation of the impact of the barrage on the local tidal range, but also the interaction between different barrages located in the same region. This way, an accurate representation of the regional hydrodynamic processes can reduce uncertainty during assessment of tidal range energy projects, which contributes to achieving an improved control strategy and reducing LCoE. Lessons regarding suitable hydrodynamic modelling for control purposes can be learned from sister renewable energies, such as is the case of wave energy conversion, where data-based modelling techniques, for example, have been considered, using either data from high-fidelity simulations [56], or experimental data obtained directly from the process [57].

The barrage models used in the literature for optimal control do not consider the environmental impact of dynamic changes in basin level. An unexplored possibility is the use of hydro-environmental models in tidal barrage operation optimisation, in which case, again, the main issue is the computational burden of the hydrodynamic model. Another possibility is to account for the environmental impact of the barrage in the OCP formulation, either in the objective function or the definition of the set of associated constraints. The study in [88], which focuses on tidal-turbine array optimisation, can serve as inspiration on how to include environmental aspects in the OCP. In particular, a multi-objective optimisation is formulated to obtain the spatial location of each turbine, where one objective function is to maximise power output, and another is to minimise the impact on water flow in the area.

6.3. Power system ancillary services

One of the main challenges that modern power systems are facing is the increase in voltage and frequency instability of electrical grids due to the large penetration of inverter-based generation, namely wind and solar power plants. Not only does the intermittency of the resources present difficulties in matching demand and supply, but also the power electronics coupling of the generators decreases the inertia and resilience of the system. The fact that tidal barrages use synchronous generators directly coupled to the grid (in the case of double-regulation turbines) can improve the voltage stability of the node. As previously mentioned in this section, using triple-regulation restricts this capability, since it requires an inverter-based coupling of the generator with the grid. On the other hand, the slow dynamics of the tidal height variations enable the use of the generators for frequency control more

effectively than in other intermittent renewables where, to perform frequency control, the available energy of the resource is underutilised. These capabilities of tidal barrages to provide ancillary services to the power grids have not been addressed in the literature on control of tidal barrages, and can potentially unlock the deployment of these types of power plants.

Another feature of tidal barrages that can be beneficial to power grids is their inherent but time-varying storage, which can be leveraged by the addition of pumping. Pumping not only provides additional operational flexibility for energy maximisation and demand-matching objectives, but could also be implemented for flattening the (local) demand curve by consuming power during low demand, which, to the best of the authors' knowledge, has not been explored in the literature. However, the performance of low-head bulb turbines as pumps needs to be further investigated. Only few of the operating tidal barrages, namely La Rance, Jiangxia and Haishan, include pumping in their operation, which does not provide enough practical evidence to establish a reliable representation of pumping in the turbines model.

6.4. Concluding remarks

To summarise the discussion in this section, a list of the main key points from this study are offered below.

- Though there is a great untapped potential for tidal range energy schemes worldwide, two main challenges need to be addressed: cost and environmental impact.
- Optimal control plays a huge role in tidal barrages, given their flexibility in operation due to the slow dynamics of the tide and the inherent storage in the basin, which allows for a wide range of operational strategies. The range of possible objective functions for tidal range plants operation has not yet been fully explored. For instance in the case of demand matching and LCoE minimisation functionals.
- The literature in tidal barrages lacks thorough studies regarding linked-basin schemes, which can be leveraged by using Haishan TPP, the existing linked-basin tidal barrage in China, as case of study.
- The hydrodynamic models used for optimal control are rather simplistic and usually over-optimistic, whereas more accurate higher-dimensional hydrodynamic models are too computationally expensive but necessary for resource and environmental impact assessment.
- Areas of potential improvement are: hydrodynamic modelling, the formulation of the OCP (by relaxing the set of simplifying assumptions considered and attacking the problem more holistically), the addition of environmental constraints, and the formulation of control co-design problems.
- There is potential for tidal barrages to offset some of the issues that modern power grids face in terms of voltage and frequency stability, but this has not been addressed in the literature.

Declaration of Competing Interest

The authors declare that they have no known competing financial interests or personal relationships that could have appeared to influence the work reported in this paper.

Data availability

No data was used for the research described in the article.

Acknowledgements

This work was supported by the Dept. of Electronic Engineering at Maynooth University under a Maynooth University Doctoral Scholarship and Science Foundation Ireland under Grant No. 18/CRT/6049. For the purpose of Open Access, the author has applied a CC BY public copyright licence to any Author Accepted Manuscript version arising from this submission. John Ringwood was supported by Science Foundation Ireland (SFI) through the MaREI Centre for Energy, Climate and Marine under Grant No. 12/RC/2302_P2. Nicolás Faedo received funding from the European Union's Horizon 2020 Research and Innovation Programme under Marie Sklodowska-Curie grant agreement No. 101024372.

References

[1] EEA. Trends and projections report 2022. European Environment Agency; 2022. Tech. Rep. 10.
[2] Hammond GP, Jones CI, Spevack R. A technology assessment of the proposed Cardiff-Weston tidal barrage, UK. Proc Inst Civil Eng - Eng Sustain 2018;171 (8): 383–401. doi:10.1680/jensu.16.00015.
[3] Charlier RH. Forty candles for the Rance River TPP tides provide renewable and sustainable power generation. Renew Sustain Energy Rev 2007;11(9):2032–57. https://doi.org/10.1016/j.rser.2006.03.015.
[4] V. Khare, C. Khare, S. Nema, P. Baredar, Introduction of tidal energy, in: Tidal Energy Systems, Elsevier, 2019, Ch. 2, pp. 41–114.
[5] Rourke FO, Boyle F, Reynolds A. Tidal energy update 2009. Appl Energy 2010;87 (2):398–409. https://doi.org/10.1016/j.apenergy.2009.08.014.
[6] Aggidis G, Feather O. Tidal range turbines and generation on the Solway Firth. Renew Energy 2012;43:9–17. https://doi.org/10.1016/j.renene.2011.11.045.
[7] Angeloudis A, Kramer SC, Avdis A, Piggott MD. Optimising tidal range power plant operation. Appl Energy 2018;212:680–90. https://doi.org/10.1016/j.apenergy.2017.12.052.
[8] Xue J, Ahmadian R, Jones O. Genetic Algorithm in tidal range schemes' optimisation. Energy 2020;200:117496. https://doi.org/10.1016/j.energy.2020.117496.
[9] Ghaedi A, Gorginpour H. Generated power enhancement of the barrage type tidal power plants. Ocean Eng 2021;226:108787. https://doi.org/10.1016/j.oceaneng.2021.108787.
[10] Kontoleontos EA, Weissenberger S. Annual energy production maximization for tidal power plants with evolutionary algorithms. Int J Fluid Mach Syst 2017;10: 264–73.
[11] Shen Y, Nyman P-O. Optimal operation of tidal plants based on nonlinear model predictive control strategy. IOP Conf Ser: Earth Environ Sci 2021;687(1):012101. https://doi.org/10.1088/1755-1315/687/1/012101.
[12] J.V. Ringwood, N. Faedo, Tidal barrage operational optimisation using wave energy control techniques, in: Proceedings of the 14th IFAC Conference on Control Applications in Marine Systems, Robotics, and Vehicles CAMS 2022, Vol. 55, Elsevier BV, Lyngby, Denmark, 2022, pp. 148–153. doi:10.1016/j.ifacol.2022.10.423.
[13] Moreira TM, de Faria JG, de Melo POV, Chaimowicz L, Medeiros-Ribeiro G. Prediction-free, real-time flexible control of tidal lagoons through Proximal Policy Optimisation: A case study for the Swansea Lagoon. Ocean Eng 2022;247:110657. https://doi.org/10.1016/j.oceaneng.2022.110657.
[14] Neill SP, Angeloudis A, Robins PE, Walkington I, Ward SL, Masters I, Lewis MJ, Piano M, Avdis A, Piggott MD, Aggidis G, Evans P, Adcock TA, Židonis A, Ahmadian R, Falconer R. Tidal range energy resource and optimization – past perspectives and future challenges. Renew Energy 2018;127:763–78. https://doi.org/10.1016/j.renene.2018.05.007.
[15] Waters S, Aggidis G. Tidal range technologies and state of the art in review. Renew Sustain Energy Rev 2016;59:514–29. https://doi.org/10.1016/j.rser.2015.12.347.
[16] N. Yates, B. Tatlock, Optimising Tidal Lagoons, in: Proceedings of the Twelfth European Wave and Tidal Energy Conference, Cork, Ireland, 2017.
[17] Todeschini G. Review of Tidal Lagoon Technology and Opportunities for Integration within the UK Energy System. Inventions 2017;2(3):14. https://doi.org/10.3390/inventions2030014.
[18] Wang ZJ, Wang ZW. A review on tidal power utilization and operation optimization. IOP Conf Ser: Earth Environ Sci 2019;240:052015. https://doi.org/10.1088/1755-1315/240/5/052015.
[19] Kadiri M, Ahmadian R, Bockelmann-Evans B, Rauen W, Falconer R. A review of the potential water quality impacts of tidal renewable energy systems. Renew Sustain Energy Rev 2012;16(1):329–41. https://doi.org/10.1016/j.rser.2011.07.160.
[20] T. Hammons, Tidal power, Proceedings of the IEEE 81 (3) (1993) 419–433.
[21] Angeloudis A, Mackie L, Piggott MD. Tidal range energy. In: Comprehensive Renewable Energy, Vol. 8. Elsevier; 2022. p. 80–103. 2nd Edition.
[22] B.B. Parker, Tidal Analysis and Prediction, NOAA Special Publication NOS CO-OPS, U.S. Department of Commerce, National Oceanic and Atmospheric Administration, National Ocean Service, Center for Operational Oceanographic Products and Services, 2007.
[23] IEA, Energy statistics data browser, https://www.iea.org/data-and-statistics/data-tools/energy-statistics-data-browser, [Accessed 27-07-2023] (2022).
[24] Xia J, Falconer RA, Lin B. Impact of different operating modes for a Severn Barrage on the tidal power and flood inundation in the Severn Estuary, UK. Appl Energy 2010;87(7):2374–91.
[25] Angeloudis A, Falconer RA. Sensitivity of tidal lagoon and barrage hydrodynamic impacts and energy outputs to operational characteristics. Renew Energy 2017; 114:337–51. https://doi.org/10.1016/j.renene.2016.08.033.

[26] Yates N, Walkington I, Burrows R, Wolf J. The energy gains realisable through pumping for tidal range energy schemes. Renew Energy 2013;58:79–84. https://doi.org/10.1016/j.renene.2013.01.039.
[27] Falconer RA, Xia J, Lin B, Ahmadian R. The Severn Barrage and other tidal energy options: Hydrodynamic and power output modeling. Sci China Ser E: Technol Sci 2009;52(11):3413–24. https://doi.org/10.1007/s11431-009-0366-z.
[28] Ward SL, Green JAM, Pelling HE. Tides, sea-level rise and tidal power extraction on the european shelf. Ocean Dyn 2012;62(8):1153–67. https://doi.org/10.1007/s10236-012-0552-6.
[29] Vandercruyssen D, Baker S, Howard D, Aggidis G. Tidal range electricity generation: A comparison between estuarine barrages and coastal lagoons. Heliyon 2022;8(11):e11381. https://doi.org/10.1016/j.heliyon.2022.e11381.
[30] Li Y, Pan D-Z. The ebb and flow of tidal barrage development in Zhejiang Province, China. Renew Sustain Energy Rev 2017;80:380–9. https://doi.org/10.1016/j.rser.2017.05.122.
[31] Chaineux M-C, Charlier RH. Women's tidal power plant Forty candles for Kislaya Guba TPP. Renew Sustain Energy Rev 2007;12(9):2515–24. https://doi.org/10.1016/j.
[32] Neill SP, Hemer M, Robins PE, Griffiths A, Furnish A, Angeloudis A. Tidal range resource of Australia. Renew Energy 2021;170:683–92. https://doi.org/10.1016/j.renene.2021.02.035.
[33] Martí Barclay V, Neill SP, Angeloudis A. Tidal range resource of the Patagonian shelf. Renew Energy 2023;209:85–96. https://doi.org/10.1016/j.renene.2023.04.001.
[34] Neto PBL, Saavedra OR, Ribeiro LAS. Optimization of electricity generation of a tidal power plant with reservoir constraints. Renewable Energy 2015;81:11–20. https://doi.org/10.1016/j.renene.2015.03.011.
[35] Mejia-Olivares CJ, Haigh ID, Angeloudis A, Lewis MJ, Neill SP. Tidal range energy resource assessment of the Gulf of California, Mexico. Renew Energy 2020;155:469–83. https://doi.org/10.1016/j.renene.2020.03.086.
[36] Department for Energy Security and Net Zero, Energy Trends March 2023, Tech. rep., Department for Energy Security and Net Zero (2023).
[37] IEA. Energy Policies of IEA Countries: United Kingdom 2019 Review. Paris: IEA; 2019. Tech. rep.
[38] Burrows R, Walkington I, Yates N, Hedges T, Chen D, Li M, Zhou J, Wolf J, Proctor R, Holt J, Prandle D. Tapping the tidal power potential of the Eastern Irish Sea. University of Liverpool and National Oceanography; 2009. Tech. Rep. Final Report, Joule Project JIRP106/03.
[39] Aggidis G, Benzon D. Operational optimisation of a tidal barrage across the Mersey Estuary using 0-D modelling. Ocean Eng 2013;66:69–81. https://doi.org/10.1016/j.oceaneng.2013.03.019.
[40] Angeloudis A, Falconer RA, Bray S, Ahmadian R. Representation and operation of tidal energy impoundments in a coastal hydrodynamic model. Renew Energy 2016;99:1103–15. https://doi.org/10.1016/j.renene.2016.08.004.
[41] Bray S, Ahmadian R, Falconer RA. Impact of representation of hydraulic structures in modelling a Severn barrage. Comput. Geosci. 2016;89:96–106. https://doi.org/10.1016/j.cageo.2016.01.010.
[42] Xue J, Ahmadian R, Jones O, Falconer RA. Design of tidal range energy generation schemes using a Genetic Algorithm model. Appl Energy 2021;286:116506. https://doi.org/10.1016/j.apenergy.2021.116506.
[43] Harcourt F, Angeloudis A, Piggott MD. Utilising the flexible generation potential of tidal range power plants to optimise economic value. Appl Energy 2019;237:873–84. https://doi.org/10.1016/j.apenergy.2018.12.091.
[44] C. Hendry, The Role of Tidal Lagoons: Final Report, Tech. rep., UK Government, London, UK (2016).
[45] Department of Energy and Climate Change, Severn Tidal Power: Feasibility Study Conclusions and Summary Report, Tech. rep., Department for Energy Security and Net Zero and Department for Business, Energy & Industrial Strategy (2010).
[46] Zhang T, Williams C, Ahmadian R, Qadrdan M, Operation Optimal. Optimal Operation of a Tidal Lagoon as a Flexible Source of Electricity. in: 2022 IEEE Power & Energy Society General Meeting (PESGM), Denver, CO, USA. 2022. p. 1–5. https://doi.org/10.1109/PESGM48719.2022.9916952.
[47] Ljung L. System Identification. Boston, MA: Birkhäuser Boston; 1998.
[48] Moreira TM, de Faria JG, de Melo POV, Medeiros-Ribeiro G. Development and validation of an AI-driven model for the La Rance tidal barrage: A generalisable case study. Appl. Energy 2023;332:120506. https://doi.org/10.1016/j.apenergy.2022.120506.
[49] Petley S, Aggidis G. Swansea Bay tidal lagoon annual energy estimation. Ocean Eng. 2016;111:348–57. https://doi.org/10.1016/j.oceaneng.2015.11.022.
[50] Egbert GD, Erofeeva SY. Efficient Inverse Modeling of Barotropic Ocean Tides. J Atmos Ocean Technol 2002;19(2):183–204. https://doi.org/10.1175/1520-0426(2002)019<0183:EIMOBO>2.0.CO;2.
[51] MIKE 21 Toolbox - Global Tide Model (2017).
[52] A. Angeloudis, R. Falconer, Operation modelling of tidal energy lagoon proposals within the Bristol channel and Severn Estuary, in: Proceedings of the 2nd International Conference on Renewable Energies Offshore, CRC Press, Lisbon, Portugal, 2016, pp. 503–512. doi:10.1201/9781315229256-61.
[53] B. Lin, R. Ahmadian, R. Falconer, Hydro-environmental modeling of proposed Severn barrage, UK, Proceedings of the Institution of Civil Engineers - Energy 163 (2010) 107–117. doi:10.1680/ener.2010.163.3.107.
[54] Ahmadian R, Falconer RA, Bockelmann-Evans B. Comparison of hydro-environmental impacts for ebb-only and two-way generation for a Severn Barrage. Comput Geosci 2014;71:11–9. https://doi.org/10.1016/j.cageo.2014.05.006.
[55] Baker AL, Craighead RM, Jarvis EJ, Stenton HC, Angeloudis A, Mackie L, Avdis A, Piggott MD, Hill J. Modelling the impact of tidal range energy on species communities. Ocean & Coast Manage 2020;193:105221. https://doi.org/10.1016/j.ocecoaman.2020.105221.
[56] Giorgi S, Davidson J, Ringwood J. Identification of wave energy device models from numerical wave tank data—part 2: Data-based model determination. IEEE Trans Sustain Energy 2016;7:1–8. https://doi.org/10.1109/TSTE.2016.2515500.
[57] Giorgi S, Davidson J, Kramer M, Ringwood J. Identification of dynamic models for a wave energy converter from experimental data. Ocean Eng 2019;183:426–36. https://doi.org/10.1016/j.oceaneng.2019.05.008.
[58] Faedo N, Dores-Piuma FJ, Giorgi G, Ringwood JV. Nonlinear model reduction for wave energy systems: a moment-matching-based approach. Nonlinear Dyn 2020;102:1215–37. https://doi.org/10.1007/s11071-020-06028-0.
[59] D. Prandle, Design of tidal barrage power schemes, Proceedings of the Institution of Civil Engineers - Maritime Engineering 126 (4) (2009) 147–153.
[60] A. Angeloudis, M. Piggott, S. Kramer, A. Avdis, D. Coles, M. Christou, Comparison of 0-D, 1-D and 2-D model capabilities for tidal range energy resource assessments, in: Proceedings of the Twelfth European Wave and Tidal Energy Conference, Cork, Ireland, 2017.
[61] Robinson IS. Tidal power from wedge-shaped estuaries — an analytical model with friction, applied to the Bristol Channel. Geophys. J. Int. 1981;65(3):611–26.
[62] Rainey RCT. The optimum position for a tidal power barrage in the Severn estuary. J Fluid Mech 2009;636:497–507. https://doi.org/10.1017/S0022112009991443.
[63] Hashemi M, Abedini M, Neill S, Malekzadeh P. Tidal and surge modelling using differential quadrature: A case study in the Bristol Channel. Coast Eng 2008;55(10):811–9. https://doi.org/10.1016/j.coastaleng.2008.02.030.
[64] Mackie L, Coles D, Piggott M, Angeloudis A. The potential for tidal range energy systems to provide continuous power: A UK case study. J Mar Sci Eng 2020;8(10):780. https://doi.org/10.3390/jmse8100780.
[65] Čož N, Ahmadian R, Falconer RA. Implementation of a Full Momentum Conservative Approach in Modelling Flow Through Tidal Structures. Water 2019;11(9):1917. https://doi.org/10.3390/w11091917.
[66] Avdis A, Candy AS, Hill J, Kramer SC, Piggott MD. Efficient unstructured mesh generation for marine renewable energy applications. Renewable Energy 2018;116:842–56. https://doi.org/10.1016/j.renene.2017.09.058.
[67] Bae YH, Kim KO, Choi BH. Lake Sihwa tidal power plant project. Ocean Eng. 2010;37(5–6):454–63. https://doi.org/10.1016/j.oceaneng.2010.01.015.
[68] Zhou J, Pan S, Falconer RA. Optimization modelling of the impacts of a Severn Barrage for a two-way generation scheme using a Continental Shelf model. Renew Energy 2014;72:415–27.
[69] Lisboa A, Vieira T, Guedes L, Vieira D, Saldanha R. Optimal analytic dispatch for tidal energy generation. Renew Energy 2017;108:371–9. https://doi.org/10.1016/j.renene.2017.02.058.
[70] Waters S, Aggidis G. A World First: Swansea Bay Tidal lagoon in review. Renew Sustain Energy Rev 2016;56:916–21. https://doi.org/10.1016/j.rser.2015.12.011.
[71] Yang C, Zheng Y, Zhou D, Ge X, Li L. Bidirectional power performance of a tidal unit with unilateral and double guide vanes. Adv Mech Eng 2013;5:415–27. https://doi.org/10.1155/2013/835051.
[72] Aggidis GA, Židonis A. Hydro turbine prototype testing and generation of performance curves: Fully automated approach. Renew Energy 2014;71:433–41. https://doi.org/10.1016/j.renene.2014.05.043.
[73] Burrows R, Walkington I, Yates N, Hedges T, Wolf J, Holt J. The tidal range energy potential of the West Coast of the United Kingdom. Appl Ocean Res 2009;31(4):229–38. https://doi.org/10.1016/j.apor.2009.10.002.
[74] Negahdari MR, Ghaedi A, Nafar M, Mohsen S. Optimal planning of the barrage type tidal power plants equipped to the hydro-pumps. Electric Power Systems Res 2023;220:109347. https://doi.org/10.1016/j.epsr.2023.109347.
[75] Lee DS, Oh S-H, Yi J-H, Park W-S, Cho H-S, Kim D-G, Eom H-M, Ahn S-J. Experimental investigation on the relationship between sluice caisson shape of tidal power plant and the water discharge capability. Renewable Energy 2010;35(10):2243–56. https://doi.org/10.1016/j.renene.2010.02.018.
[76] Liberzon D. Calculus of Variations and Optimal Control Theory: A Concise Introduction. Princeton University Press; 2011.
[77] L. Mackie, F. Harcourt, A. Angeloudis, M. Piggott, Income optimisation of a fleet of tidal lagoons, in: Proceedings of the Thirteenth European Wave and Tidal Energy Conference, Naples, Italy, 2019.
[78] Angeloudis A, Kramer SC, Hawkins N, Piggott MD. On the potential of linked-basin tidal power plants: An operational and coastal modelling assessment. Renew Energy 2020;155:876–88. https://doi.org/10.1016/j.renene.2020.03.167.
[79] Angeloudis A, Ahmadian R, Falconer RA, Bockelmann-Evans B. Numerical model simulations for optimisation of tidal lagoon schemes. Appl Energy 2016;165:522–36. https://doi.org/10.1016/j.apenergy.2015.12.079.
[80] Xue J, Ahmadian R, Falconer R. Optimising the operation of tidal range schemes. Energies 2019;12(15):2870. https://doi.org/10.3390/en12152870.
[81] Ryrie S. An optimal control model of tidal power generation. Appl Math Model 1995;19(2):123–6. https://doi.org/10.1016/0307-904X(94)00012-U.
[82] Prandle D. Simple theory for designing tidal power schemes. Adv Water Resour 1984;7(1):21–7. https://doi.org/10.1016/0309-1708(84)90026-5.
[83] Wales D. Exploring Energy Landscapes. Annual Review of Physical Chemestry 2018;69:401–25. https://doi.org/10.1146/annurev-physchem-.
[84] H. Ross, M. Hall, D.R. Herber, J. Jonkman, A.K. Sundarrajan, T.T. Tran, A. Wright, D. Zalkind, N. Johnson, Development of a Control Co-Design Modeling Tool for Marine Hydrokinetic Turbines, in: Proceedings of the ASME 2022 International Mechanical Engineering Congress and Exposition, Vol. 6, Ohio, USA, 2022.
[85] Cohen J, Kane MB, Marriott A, Ollivierre F, Govertsen K. Economic Controls Co-Design of Hybrid Microgrids with Tidal/PV Generation and Lithium-Ion/Flow Battery Storage. Energies 2023;16(6):2761. https://doi.org/10.3390/en16062761.

[86] Peña-Sanchez Y, García-Violini D, Ringwood JV. Control co-design of power take-off parameters for wave energy systems. In: Joint 9th IFAC Symposium on Mechatronic Systems and 16th International Conference on Motion and Vibration Control, California, USA, Vol. 55; 2022. p. 311–6.
[87] Mallemaci V, Mandrile F, Rubino S, Mazza A, Carpaneto E, Bojoi R. A comprehensive comparison of Virtual Synchronous Generators with focus on virtual inertia and frequency regulation. Electric Power Syst Res 2021;201:107516. https://doi.org/10.1016/j.epsr.2021.107516.
[88] du Feu R, Funke S, Kramer S, Culley D, Hill J, Halpern B, Piggott M. The trade-off between tidal-turbine array yield and impact on flow: A multi-objective optimisation problem. Renew Energy 2017;114:1247–57. https://doi.org/10.1016/j.renene.2017.07.081.